CIVIL ENGINEERING STUDIES
Illinois Center for Transportation Series No. 23-012
UILU-ENG-2023-2012
ISSN: 0197-9191

Measuring Transport Properties of Portland Cement Concrete Using Electrical Resistivity

Prepared By
Julie Ann Hartell
Hang Zeng
Texas A&M University

Matthew O'Reilly
University of Kansas

Research Report No. FHWA-ICT-23-011

A report of the findings of

ICT PROJECT R27-208
Measuring Transport Properties of Portland Cement Concrete Using Electrical Resistivity

https://doi.org/10.36501/0197-9191/23-012

Illinois Center for Transportation

August 2023

TECHNICAL REPORT DOCUMENTATION PAGE

1. Report No. FHWA-ICT-23-011	**2. Government Accession No.** N/A	**3. Recipient's Catalog No.** N/A
4. Title and Subtitle Measuring Transport Properties of Portland Cement Concrete Using Electrical Resistivity		**5. Report Date** August 2023 **6. Performing Organization Code** N/A
7. Authors Julie Ann Hartell, Matthew O'Reilly, and Hang Zeng		**8. Performing Organization Report No.** ICT-23-012 UILU-2023-2012
9. Performing Organization Name and Address Illinois Center for Transportation Department of Civil and Environmental Engineering University of Illinois at Urbana-Champaign 205 North Mathews Avenue, MC-250 Urbana, IL 61801		**10. Work Unit No.** N/A **11. Contract or Grant No.** R27-208
12. Sponsoring Agency Name and Address Illinois Department of Transportation (SPR) Bureau of Research 126 East Ash Street Springfield, IL 62704		**13. Type of Report and Period Covered** Final Report 8/16/19–8/15/23 **14. Sponsoring Agency Code**

15. Supplementary Notes
Conducted in cooperation with the U.S. Department of Transportation, Federal Highway Administration.
https://doi.org/10.36501/0197-9191/23-012

16. Abstract
Although classification tables based on susceptibility to chloride ion permeability are recommended in AASHTO T 358, the classification levels with respect to durability parameters may or may not be adequate. Of interest for concrete pavement performance, this study verifies the recommended classification levels against standard durability testing such as corrosion, salt scaling, and freeze-thaw. The researchers conducted corrosion, salt scaling, and freeze-thaw durability tests in parallel with electrical surface resistivity testing to compare performance classifications for each method. Twenty-four mixture designs were evaluated. The designs vary in water-to-cementitious material ratio (0.4, 0.45, and 0.5 w/cm ratio), supplementary cementitious material type (100% ordinary Portland cement, 20% Class C fly ash, 40% Grade 100 slag cement, and 8% silica fume replacements), and air content (air entrained and non-air entrained). The results of the experimental study indicate that there is no clear relationship between concrete electrical conductivity and durability performance based on standard methods of testing. It may not be appropriate for the determination of durability performance of a concrete mixture for concrete pavement construction. However, the test method does present advantages, as mixtures of similar composition and design can yield the same results over time under standardized curing. Here, resistivity-time curves could be a useful tool as part of a quality control and quality assurance program to ensure consistency in concrete delivery during construction.

17. Key Words Concrete, Electrical Resistivity, Freeze-Thaw Durability, Corrosion Performance	**18. Distribution Statement** No restrictions. This document is available through the National Technical Information Service, Springfield, VA 22161.

19. Security Classif. (of this report) Unclassified	**20. Security Classif. (of this page)** Unclassified	**21. No. of Pages** 53 + appendices	**22. Price** N/A

Form DOT F 1700.7 (8-72) **Reproduction of completed page authorized**

ACKNOWLEDGMENT, DISCLAIMER, MANUFACTURERS' NAMES

This publication is based on the results of **ICT-R27-208: Measuring Transport Properties of Portland Cement Concrete Using Electrical Resistivity**. ICT-R27-208 was conducted in cooperation with the Illinois Center for Transportation; the Illinois Department of Transportation; and the U.S. Department of Transportation, Federal Highway Administration.

Members of the Technical Review Panel (TRP) were the following:

- James Krstulovich, TRP Chair, Illinois Department of Transportation
- Michael Ayers, Illinois Concrete Pavement Association
- Dennis Bachman, Federal Highway Administration
- Julie Beran, Illinois Department of Transportation
- Craig Cassem, Federal Highway Administration
- Mike Copp, Illinois Department of Transportation
- Kevin Finn, Illinois Department of Transportation
- Dan Gancarz, Illinois Tollway
- Stephen Jones, Illinois Department of Transportation
- Kelly Morse, Illinois Department of Transportation
- Irene Pantoja, Federal Highway Administration
- John Senger, Illinois Department of Transportation
- Megan Swanson, Illinois Department of Transportation
- Steve Worsfold, S.T.A.T.E. Testing, LLC

TABLE OF CONTENTS

LIST OF FIGURES

LIST OF TABLES

CHAPTER 1: INTRODUCTION

The durability of concrete is widely recognized to be controlled by the ingress of detrimental agents. Here, preventing penetration of water, oxygen, carbon dioxide, and salts is key to maximize material performance and longevity (Neithalath & Jain, 2010). The rapid chloride permeability test (RCPT) and now resistivity testing are used widely to assess the quality of a concrete mixture based on its performance in resisting ionic flow (Kessler et al., 2005; Kessler et al., 2008; Nadelman & Kurtis, 2014). In fact, many people feel that the permeability of concrete is more important than its strength. The challenge has been that permeability was neither measured nor specified by engineers because of the inherent challenges associated with procedural and material variability. This thought has recently changed with the widespread introduction of the resistivity meter.

Resistivity meters are used to measure the flow of electrons through concrete. They take only a few seconds to run and show good correlation to the RCPT and the bulk diffusion test. The test has been standardized by both ASTM C1760 and AASHTO T 358. However, with an increase in body of knowledge on the test method, correlations between ionic- and electrical-based transport properties may have been determined, but how both relate to physical transport mechanisms is still a subject of debate. Physical ingress of aggressive agents into concrete is an underlying cause of common durability concerns for concrete used in the construction of surface transportation infrastructure, so it is of importance to understand the various test principles measuring transport properties and their efficacy. The rapidity and simplicity of electrical resistivity testing make the method an ideal candidate for assessing the performance of a concrete material as well as for quality control of concrete mixtures.

REVIEW OF ELECTRICAL RESISTIVITY METHOD

Research has demonstrated that nondestructive electrical methods such as the surface resistivity and bulk resistivity methods may be adequate in determining the susceptibility of a concrete mixture to chloride ion penetrability (CIP) through a comparative relationship with the ASTM C1202 standard for RCPT (Kessler et al., 2005; Rupnow & Icenogle, 2011; Spragg et al., 2013).

In the past two decades, methods were developed such as the FM 5-578, AASHTO TP 95-11 (2014), and ASTM C1760–12. The extensive body of research led to the development of the AASHTO standard T 358, in which recommendations for classification are of high to negligible CIP (Table 1) with regards to apparent electrical resistivity performed on a 100 × 200 mm (4 x 8 in.) cylinder. In this case, a higher resistivity value would correspond to improved CIP performance. However, many factors may affect the outcome of a test and must be considered to ensure adequacy of the results.

Table 1. Chloride Ion Penetrability Classification According to AASHTO T 358

Chloride Ion Penetrability	AASHTO T 358 (KΩ.cm)
High	< 12
Moderate	12 to 21
Low	21 to 37
Very Low	37 to 254
Negligible	> 254

Factors Affecting Test Accuracy

Past investigations demonstrate that resistivity measurements are influenced mainly by the microstructure of concrete, pore solution conductivity, saturation condition, and temperature of concrete (Spragg et al., 2013). However, there are many factors that may influence the accuracy of the measured values due to the test principle itself (procedural variability) and the inherent variability of concrete materials. The following sections provide a summary of main recommendations from previous research activities.

Procedural Variability

Sample Geometry and Probe Spacing

When measuring resistivity of concrete, it is assumed that the material is homogeneous. However, the aggregate/mortar interface will influence the result of a measurement. To minimize the influence of the aggregate interface (maximum size), a large probe spacing should be considered. Typically, a probe spacing of 38 mm (1.5 in.) is used for a maximum aggregate size of 25 mm (1 in.), corresponding to the standard resistivity meter probe configuration in North America. This spacing is also adequate for use on a 100 × 200 mm (4 x 8 in.) cylinder. The proposed CIP classifications in AASHTO T 358 are based on the measured resistivity for these conditions.

When measuring the resistivity of a cylinder of varying size, the apparent resistivity can be factored to determine the true resistivity of the concrete material (equation 1 in Figure 1). The correction factor K (Figure 1 and 2) must be applied to account for geometrical effects such as the curvature of samples (Morris et al., 1996). Here, proper selection of probe spacing in accordance with cylinder geometry is of importance. To minimize the influence of geometrical effects, it is preferable that the determined K factor fall toward the horizontal asymptote of the curve. A small L/a ratio (i.e., small cylinder length and large probe spacing) will decrease the reliability of the calculated resistivity. As such, probe spacing and cylinder size must be examined carefully and determined when evaluating a concrete mixture. When taking a resistivity measurement of a slab with a large surface area, the resistivity measured does not require a correction.

$$\rho_{real} = \rho_{measure}/K \qquad \text{Eq. 1}$$

Figure 1. Equation. Determination of true resistivity of concrete from measured specimen apparent resistivity and correction factor K.

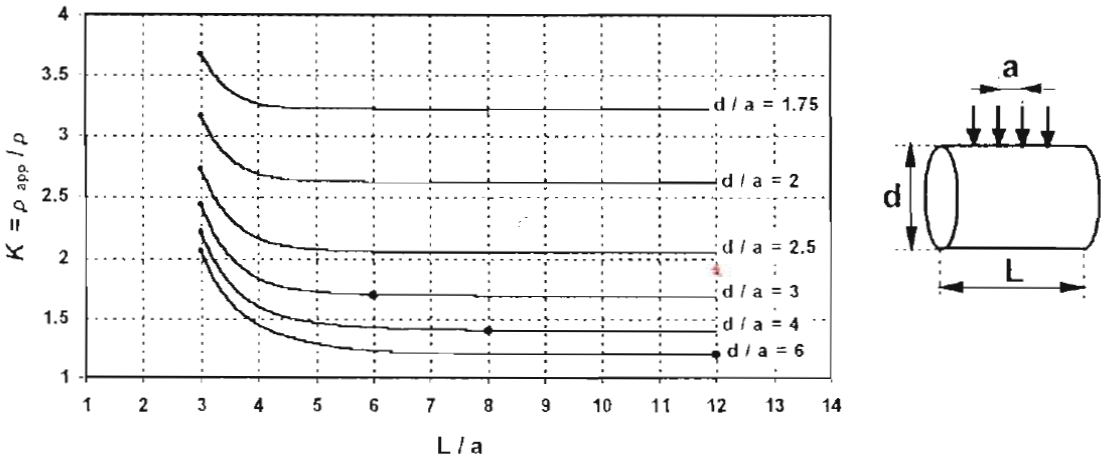

Figure 2. Graph. Determination of concrete resistivity using a cell constant or geometry factor (K).

Source: Morris et al. (1996)

Edge Effect

When taking a measurement, it is important to position the probe at the center of the specimen, away from the edges. Due to a change in current density, the resistivity value will increase if the measurement is taken near the edge of a specimen (Figure 3). Therefore, adequate probe spacing for the length of the specimen and placement at the center of a cylinder sample is of importance (Morris et al., 1996; Kessler et al., 2005).

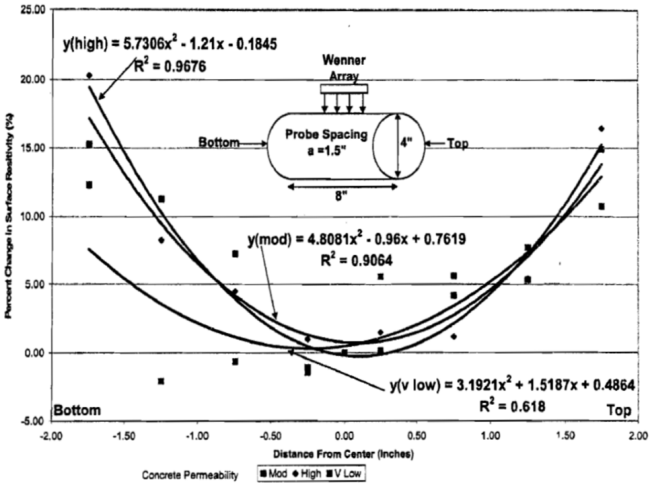

Figure 3. Graph. Influence of probe position on cylinder.

Source: Morris et al. (1996)

Surface Wetting

A surface resistivity reading is valid only when the surface is wet. The reading will be lower if the surface is allowed to dry for several minutes (Kessler et al., 2005). Therefore, a measurement should

be taken within the first 5 minutes after a sample is taken out of a moist curing chamber or immersion tank. Excessive surface water (film of water) may result in an increase in resistivity due to a favorable electrical path through the film of water. Careful surface preparation must be taken to ensure optimal probe contact with the surface as well as reading. Certain meters require probes to be pre-saturated or to use a coupling gel to ensure electrical conductivity. Both should be kept minimal to provide surface contact alone.

Curing Method

Florida DOT restricts curing to one method (moist curing), because moist curing produces, on average, higher values (9.7%) compared to limewater curing (Kessler et al., 2005). Due to leaching of ions, the storage solution and solution volume to sample ratio seem to effect resistivity values. A solution/sample ratio of 2.0 is recommended (Spragg et al., 2013). In line with Florida DOT, the Kansas test method specifies a result multiplier (1.1) for limewater curing (KT-79). However, this 10% difference was not noticed in the study by Gulrez and Hartell (2018).

Curing Temperature

Curing temperature will affect the degree in maturity at a given age and, therefore, should be specified (Spragg et al., 2013). Hartell (2020) found that if cured within the ASTM C511 recommended temperature range of 23.0 ± 2.0 °C (73°F ± 3°F), there is not a significant difference in the measurement. However, if cured at temperatures outside the range, the resistivity value will be affected. Mixtures containing fly ash were more susceptible than ordinary Portland cement (OPC) concrete mixtures for a narrow range outside ASTM limits (Gulrez & Hartell, 2017; Hartell, 2020).

Sample/Ambient Testing Temperature

The conductivity of an electrolyte solution changes with temperature. Generally, the conductivity-temperature relationship is linear and expressed as a percentage per 1°C. Polder (2000) reported a general linear relationship of 3% and 5% change in values for every 1°C in temperature difference for moist and dry concrete, respectively. Spragg et al. (2013) reported that a relatively narrow range in temperature (e.g., ± 2°C) should be specified.

Hartell (2020) found that for ambient laboratory conditions, 23°C ± 2°C (73°F ± 3°F), the influence of ambient temperature and cylinder temperature is not significant. However, outside of the temperature range, the influence of a cylinder's surface temperature may have an adverse effect on the measurement. The correction factor was approximately ±1%–2% change in resistivity per 1°C from the datum value 23°C. This is valid for a temperature range of ±2°C from the datum (23°C). The percent change is also dependent on the supplementary cementitious material (SCM) type and quantity (Hartell, 2020). Therefore, testing in a temperature-controlled laboratory environment is recommend to ensure comparable results.

Operator Statistical Scatter

For the same samples, conditions, and apparatus, the results indicate that operator-induced variability is minimal, and scatter is due to intrinsic differences within the cylindrical concrete specimen because concrete is a heterogenous material (Kessler et al., 2005).

For a sample of three cylinder replicates, the bulk electrical conductivity test precision statement for single-operator variability is 9.2% coefficient of variation (ASTM C 1790). For FM5-578, the surface resistivity test precision statement for single-operator variability is 8.2% coefficient of variation. This value is 6.4% for AASHTO T 358.

Variability Due to Mixture Design

Chemistry of Cementitious Material

The conductivity of an electrolyte changes with ionic strength and ionic type. As such, the resistivity of a concrete sample changes with pore solution chemistry. Any known phenomenon that alters the pore solution chemistry will affect the resistivity measurement. Cementitious replacement with SCMs and the percent replacement will influence the resistivity measurement.

Water-to-Cementitious Material Ratio

For concrete mixtures between a water-to-cementitious material (w/cm) ratio of 0.4 and 0.5, a change in water content can significantly change the resistivity of concrete. Over a 0.5 w/cm ratio, it becomes difficult to discern concrete mixtures of higher water content (Figure 4) (Hartell, 2020; Gulrez & Hartell, 2018).

Admixture Addition

In standard dosing, the addition of air entrainment does not significantly affect the resistivity measurement. The combined addition of a water-reducing agent and an air-entraining agent may have a marginal effect for concrete containing SCMs and of higher w/cm ratio (Hartell, 2019).

Aggregate Gradation and Type

For a similar paste type and content, small changes in coarse aggregate gradation and maximum size may not significantly alter the resistivity value of a concrete mixture. If the paste content is changed, a small increase in resistivity is expected with an increase in paste content. Aggregate minerology may also affect resistivity for various cementitious materials (Gulrez & Hartell, 2019).

Correlation with Durability Parameters

The resistivity method can be an effective tool, if performed correctly and with an understanding of its capabilities. The meaning of the generated test result for a given concrete mixture is still not well understood. Although classification tables based on susceptibility to chloride ion permeability are recommended in AASHTO T 358, the method lacks clear understanding on how it correlates to actual durability testing such as corrosion, salt-scaling, and freeze-thaw standard tests. Such parameters are of importance when designing a well-performing concrete mixture for pavement construction.

The literature provides insufficient knowledge to properly categorize concrete mixtures based on resistivity testing. Hartell (2020) determined that w/cm ratio and SCM addition are the prevailing parameters affecting the outcome of a resistivity test. Meanwhile, through statistical analysis, aggregate gradation type and air entrainment may not have a significant effect on resistivity with respect to their control for a given w/cm ratio. Variations in fly ash sources did not yield significant

differences in behavior during the first 28 days of testing as well as Types I/II and Type III cement investigated. In the first 28 days of testing, a mixture containing up to 25% Class C fly ash may not be discerned from an OPC control. As such, it is recommended that mixtures containing SCMs should be evaluated at a later age, such as at 56 days or 91 days, to capture pore refinement benefits associated with SCM use in concrete. Similar behaviors were found for slag cement and silica fume SCM replacements (Hartell & Shults, 2018). However, the length of testing required to achieve a meaningful result according to AASHTO T 358 is impractical.

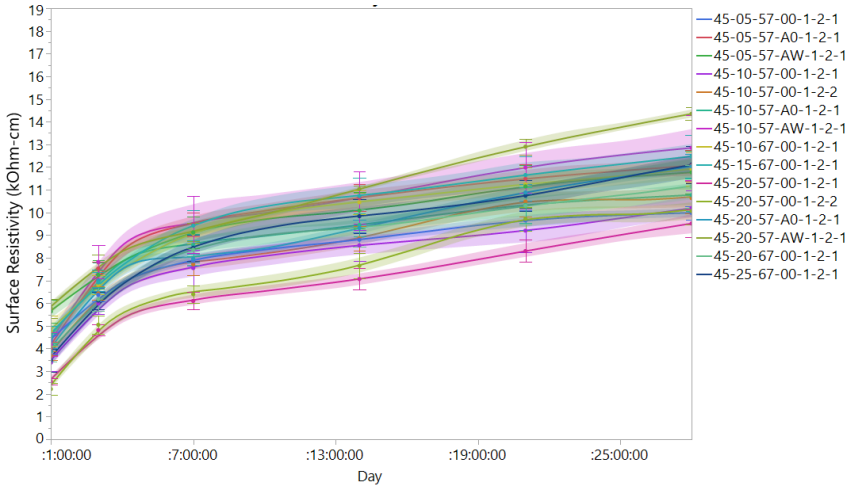

Figure 4. Graph. Resistivity results of a parametric investigation for mixtures with a 0.45 w/cm ratio containing varying mix design parameters.

Source: Hartell (2020)

From a study conducted by Hartell (2020), Figure 4 presents an example of the spread in resistivity results for a mixture design with a 0.45 w/cm ratio with varying Class C fly ash content, aggregate size and type, cement type, and admixture addition. Statistically speaking, none of the mixtures can be discerned from one another based on a single resistivity value prior to 28 days. This observable resistivity behavior is similar for every w/cm ratio evaluated except with a discernable increase (0.40 w/cm ratio) or decrease (0.50 w/cm ratio) in resistivity. Mixtures of 0.50 w/cm to 0.60 w/cm ratios are statistically similar and cannot be differentiated using resistivity testing within the first 56 days of testing. This fact poses a problem when designing a concrete pavement mixture based on performance measures. Optimization in SCM replacements and admixture additions may not be reflected through resistivity testing. Implementation of AASHTO TT 84 must be evaluated carefully when it comes to resistivity testing as a means to determine the performance of a mixture.

OBJECTIVE OF THE STUDY

The aim of the study is to investigate the existence of correlations between resistivity testing and standardized methods for durability testing of concrete. The research plan includes a series of durability tests commonly performed to assess the performance of a mixture design for concrete pavement construction. The results are compared to companion electrical surface resistivity measurements to identify any existing relationships. The second objective of the study was to

determine the efficacy of conducting a resistivity test by four different laboratories. The result interpretation of the interlaboratory trial conducted by four participating districts can provide an indication of repeatability of the test method and operator performance between laboratories. Lastly, a series of mixture designs and associated resistivity testing performed by an independent laboratory is evaluated to identify potential characteristics that can aid in the successful implementation of resistivity testing as a means to evaluate the performance of concrete material for pavement construction.

CHAPTER 2: EXPERIMENTAL PROGRAM

To accomplish the objectives of this research project, this chapter introduces an experimental program, including information on materials tested and specimen preparation as well as the different standard testing procedures followed.

MATERIALS

Cement and Supplementary Cementitious Materials

A Type I Portland cement, specified ASTM C150, from Central Plains Cement Company was used. A Class C fly ash from Hugo Plant in Oklahoma, a Grade 100 slag cement, and a silica fume were used in the mixtures prepared for the durability study. Cement bags and other SCMs received from various sources were sealed in 5-gallon buckets and were stocked in a clean and dry area inside the Center for Infrastructure Renewal Lab at Texas A&M University System.

Aggregates

The concrete mixtures were prepared with Quapaw (#57) coarse aggregate and dover sand per ASTM C33. The coarse aggregates were stocked outside in the yard of the Center for Infrastructure Renewal Lab at Texas A&M University System. As per ASTM C127 and C128, the specific gravity and absorption for the coarse aggregate are 2.66 and 0.92%, respectively, and the specific gravity and absorption for the fine aggregate are 2.60 and 0.64%, respectively.

Chemical Admixtures

For comparative analysis, some of the concrete mixtures were prepared with the addition of chemical admixtures, such as the air-entraining admixture MasterAir AE 90.

Mixture Design

For durability testing, 24 mixture designs were prepared. The parametric investigation comprises mixtures of varying w/cm ratios, OPC cement replacement with different SCMs, and the addition of an air-entraining admixture. Three water-to-cementitious material ratios were evaluated: 0.40, 0.45, and 0.50. A 100% OPC and three SCM replacements were prepared: 20% fly ash, 40% slag, and 8% silica fume. Both sets of mixtures were prepared with and without an air-entraining admixture. Table 2 provides the mixture designs. The nomenclature described in Table 3 was adopted and used hereafter for the different concrete mixtures.

Table 2. Concrete Mixture Design Quantities

Description	w/cm Ratio	OPC (lb/yd^3)	SCM (lb/yd^3)	Coarse Agg. (lb/yd^3)	Fine Agg. (lb/yd^3)	Water (lb/yd^3)	Air Entrainer (mL yd^3)
Plain OPC	0.4	611	0	1850	1250	245	0
Plain OPC	0.45	611	0	1850	1250	275	0
Plain OPC	0.5	611	0	1850	1250	306	0
OPC + Air	0.4	611	0	1850	1250	245	270
OPC + Air	0.45	611	0	1850	1250	275	270
OPC + Air	0.5	611	0	1850	1250	306	270
20% Fly Ash	0.4	488.8	122.2	1850	1250	245	0
20% Fly Ash	0.45	488.8	122.2	1850	1250	275	0
20% Fly Ash	0.5	488.8	122.2	1850	1250	306	0
20% Ash + Air	0.4	488.8	122.2	1850	1250	245	270
20% Ash + Air	0.45	488.8	122.2	1850	1250	275	270
20% Ash + Air	0.5	488.8	122.2	1850	1250	306	270
40% Slag	0.4	366.6	244.4	1850	1250	245	0
40% Slag	0.45	366.6	244.4	1850	1250	275	0
40% Slag	0.5	366.6	244.4	1850	1250	306	0
40% Slag + Air	0.4	366.6	244.4	1850	1250	245	270
40% Slag + Air	0.45	366.6	244.4	1850	1250	275	270
40% Slag + Air	0.5	366.6	244.4	1850	1250	306	270
8% Silica Fume	0.4	562.1	48.9	1850	1250	245	0
8% Silica Fume	0.45	562.1	48.9	1850	1250	275	0
8% Silica Fume	0.5	562.1	48.9	1850	1250	306	0
8% Silica Fume + Air	0.4	562.1	48.9	1850	1250	245	270
8% Silica Fume + Air	0.45	562.1	48.9	1850	1250	275	270
8% Silica Fume + Air	0.5	562.1	48.9	1850	1250	306	270

Table 3. Nomenclature for Different Mixtures

Mixture ID	Cementitious Material	Air Entrainer
OPC-0-0	100% OPC	No
OPC-1-0	100% OPC	Yes
FA-0-0	80% OPC + 20% fly ash	No
FA-1-0	80% OPC + 20% fly ash	Yes
SG-0-0	60% OPC + 40% slag	No
SG-1-0	60% OPC + 40% slag	Yes
SF-0-0	92% OPC + 8% silica fume	No
SF-1-0	92% OPC + 8% silica fume	Yes

SPECIMEN MIXING, CURING, AND CONDITIONING

Twenty-four concrete mixtures were prepared at CIR laboratory facilities. Concrete mixing and specimen casting were accomplished according to the ASTM C192 procedure in a controlled laboratory environment.

Standard fresh concrete property tests, such as slump (ASTM C143), unit weight (ASTM C138), and percent air content (ASTM C231), were performed on individual batches to maintain the quality and

consistency of concrete mixtures. If a mixture did not meet the anticipated design values, then the mixture was discarded.

From each concrete batch, three cylindrical specimens Ø 100 × 200 mm (Ø 4 × 8 in.), two slab specimens 200 × 300 × 75 mm (8 × 12 × 3 in.), and two prism specimens 75 × 100 × 400 mm (3 × 4 × 16 in.) were cast. The specimens were cast in a standard manner and consolidated using external vibration. They were demolded after 24 hours of initial curing.

Afterwards, the cylinders were cured in saturated limewater buckets stored in a moist curing room maintained at 23.0°C ± 2.0°C (73.5°F ± 3.5°F). They remained immersed for the entirety of the test period of 98 days. The prisms were immersion cured for 14 days prior to the start of freeze-thaw testing.

The slabs were moist cured in the same chamber for 28 days. After 28 days, the slab samples were taken out from the curing room and allowed to air dry in an environmental chamber maintained at 50% relative humidity and 23.0°C ± 2.0°C (73.5°F ± 3.5°F) for 14 days. Thereafter the slabs were ponded with a 3% sodium chloride solution for seven days prior to the start of the scaling test.

SURFACE RESISTIVITY TESTING

Surface resistivity testing was conducted following AASHTO T 358 (Figure 5). The measurements were taken with a Proceq Resipod four-point resistivity meter with a fixed probe spacing of 38 mm (1.5 in.). A set of three concrete cylinders were prepared from each concrete mixture. After demolding, each sample was marked with four lines on the longitudinal sides of the cylinder at 0, 90, 180, and 270 degrees. Then, four different points on each line were marked corresponding to the resistivity probe placement. A total of eight measurements along the four axes for each specimen were recorded. Surface resistivity was measured according to the following schedule: day 1, 3, 7, 14, 21, 28, 42, 56, 70, 84, and 98.

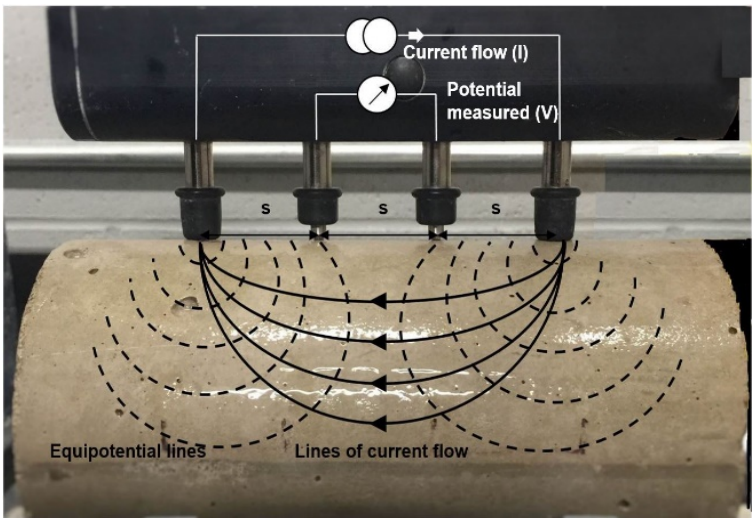

Figure 5. Photo. Illustration of surface resistivity test principle.

Source: Hartell & Shults (2018)

FREEZE-THAW DURABILITY TESTING

Freezing and Thawing Exposure Regimen

For this study, procedure B defined in ASTM C666 was followed. Temperature cycles were accomplished by alternating storage of prism specimens in an environmental chamber maintained at −18°C ± 2°C and another maintained at 4°C ± 2°C. Each freeze-thaw cycle was performed daily, where samples thawed for 8 hours in water and froze for 16 hours in air. The specimens were placed on a wire cart during the freezing cycle and in a plastic container filled with water during the thawing cycle (Figure 6).

(a) (b)

Figure 6. Photo. Prisms exposed to (a) freezing temperature in air and (b) thawing in water.

Resonant Frequency Testing

The ASTM C215 standard method was performed to determine the fundamental resonant frequency of prism specimens subjected to cycle changes in temperature. This value is related to a material's dynamic modulus of elasticity. A change in this value may be an indication of material degradation. Therefore, the relative dynamic modulus of elasticity was used to assess the damage degree of the specimens at intervals of 10 cycles of freeze-thaw exposure. The test was performed until the relative dynamic modulus of elasticity reached 60% of its initial value or 300 cycles, whichever occurred first (ASTM C666).

SALT-SCALING DURABILITY TESTING

A modified BNQ NQ 2621-900 standard method of salt scaling test was followed (Hooton & Vassilev, 2012). The procedure requires 50 freezing and thawing cycles, where each cycle consists of 16 hours ± 1 hour of freezing at −18°C ± 2°C, followed by 8 hours ± 1 hour of thawing in ambient laboratory conditions at 21.5°C ± 2.5°C. During this time, the slab surface is ponded with a 3% sodium chloride solution. The brine pond was contained by a dike made with polystyrene foam insulation board. The foam board covered all four sides of the slab as well as its bottom, serving as insulation to prevent a freezing front for other slab surfaces. During temperature exposure, the top surfaces of the slabs were covered with a plastic sheet to prevent solution evaporation (Figure 7). After five freeze-thaw cycles, each specimen's surface was rinsed, and any loose material was carefully collected by filtering the rinse with an 80 µm filter paper. In addition, photographs of each specimen's top surface were taken to visually monitor the change in surface degradation. Next, the pond was replenished and subjected to the next five cycles. At increments of five cycles, the cumulative mass loss was measured until 50 temperature cycles or until failure (average mass loss above 0.5 kg/m^2).

Figure 7. Photo. Salt-scaling slab specimen on wire cart.

MODIFIED RAPID MACROCELL TEST

Materials

The aggregates, cementitious materials, and admixtures used for the mortar-wrapped macrocell specimens are identical to those used for the other specimens described in this report, with the exception that coarse aggregates were not used in the mortar. Table 4 presents the resulting mortar mix designs.

Table 4. Mix Proportions for Mortar-Wrapped Rapid Macrocell Test

Description	w/cm Ratio	OPC (lb)	SCM (lb)	Fine Agg. (lb)	Water (lb)	Air Entrainer (mL)
Plain OPC	0.4	2.37	0.00	4.93	0.87	0.00
Plain OPC	0.45	2.30	0.00	4.78	0.96	0.00
Plain OPC	0.5	2.23	0.00	4.63	1.05	0.00
OPC + Air	0.4	2.25	0.00	4.68	0.83	0.60
OPC + Air	0.45	2.19	0.00	4.55	0.91	0.60
OPC + Air	0.5	2.13	0.00	4.42	1.00	0.60
20% Fly Ash	0.4	1.88	0.47	4.89	0.87	0.00
20% Fly Ash	0.45	1.83	0.46	4.75	0.95	0.00
20% Fly Ash	0.5	1.77	0.44	4.61	1.04	0.00
20% Ash + Air	0.4	1.79	0.45	4.65	0.83	0.60
20% Ash + Air	0.45	1.74	0.43	4.52	0.91	0.60
20% Ash + Air	0.5	1.69	0.42	4.39	0.99	0.60
40% Slag	0.4	1.41	0.94	4.89	0.87	0.00
40% Slag	0.45	1.37	0.91	4.75	0.95	0.00
40% Slag	0.5	1.33	0.89	4.60	1.04	0.00
40% Slag + Air	0.4	1.34	0.90	4.65	0.83	0.60
40% Slag + Air	0.45	1.30	0.87	4.52	0.91	0.60
40% Slag + Air	0.5	1.27	0.84	4.39	0.99	0.60
8% Silica Fume	0.4	2.17	0.19	4.90	0.87	0.00
8% Silica Fume	0.45	2.10	0.18	4.75	0.96	0.00
8% Silica Fume	0.5	2.04	0.18	4.61	1.04	0.00
8% Silica Fume + Air	0.4	2.06	0.18	4.66	0.83	0.60
8% Silica Fume + Air	0.45	2.00	0.17	4.52	0.91	0.60
8% Silica Fume + Air	0.5	1.94	0.17	4.39	0.99	0.60

Test Specimens

The mortar-wrapped macrocell specimen is a modified version of the rapid macrocell test outlined in the Annex of ASTM A955 and is presented in Figure 8. A single rapid macrocell specimen consists of an anode and a cathode. The test specimen consists of two containers, each filled to a depth of 89 mm (3.5 in.) with a simulated pore solution. The anode half of the specimen, where corrosion is induced, has the equivalent of a 15% (6.04 molal ion) sodium chloride solution added to the pore solution to simulate chloride-contaminated concrete. The cathode has a pore solution with no chlorides. One liter of pore solution consists of 974.8 g of distilled water, 18.81 g of potassium hydroxide, and 17.87 g of sodium hydroxide. Air is bubbled into the cathode solution to remove carbon dioxide, ensuring an adequate supply of oxygen required for the cathodic reaction. Deionized water is added to the containers as needed to maintain a constant volume of the solution. The solutions are changed every five weeks to limit the effects of carbonation. The anode and cathode are electrically connected across a 10 ohm resistor. A potassium chloride salt bridge provides an ionic connection between the anode and the cathode.

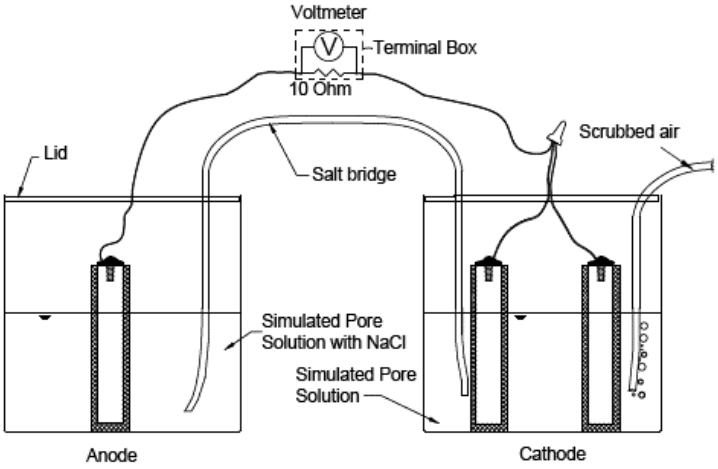

Figure 8. Sketch. Mortar-wrapped rapid macrocell test.

The fabrication of rapid macrocell specimens proceeds as follows. No. 5 reinforcing bars are cut to a length of 127 mm (5 in.) with a band saw. One end of each bar is drilled and tapped to receive a 10 mm (3/8 in.) long stainless-steel screw with 10-24 threading. Bars are soaked in acetone for a minimum of two hours and cleaned to remove any oil. To cast the specimens, bars are secured to a plywood base using a 10-24 machine screw: a 140 mm (5.5 in.) length of 25 mm (1 in.) A Schedule 10 PVC pipe is centered around each bar and secured to the plywood base with caulk (Figure 9). A minimum of 15 bars (five specimens) were planned for each mortar mixture. In some cases, damage to specimens or limited materials resulted in sufficient bars for only four specimens.

Specimens are cast with the mortar mixtures outlined in the previous section. Specimens are filled in three layers, and external vibration is used to consolidate the mortar between each layer. Specimens are covered in plastic for 24 hours after casting, at which time they are removed from the PVC and plywood and cured in a moist curing room for an additional six days. Specimens dry cure for 21 days prior to the start of testing at 28 days after casting.

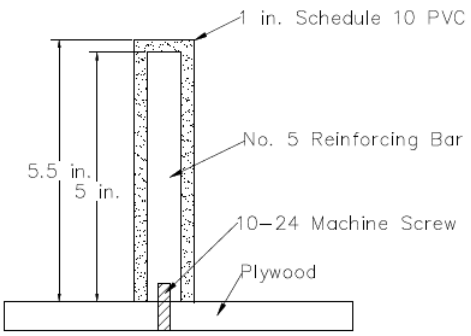

Figure 9. Sketch. Mortar-wrapped rapid macrocell form.

Prior to testing, 16-gauge wire leads are connected to the test bars using a 10-24 × 10 mm (3/8 in.) stainless-steel screw. Multiple coats of epoxy are applied to the electrical connection to protect it from corrosion. Mortar-wrapped bars are placed upright in the plastic containers, and pore solution is

added to a depth of 140 mm (3.5 in.), exposing 75 mm (3 in.) of bar to the solution. Bars are connected to a terminal box at the start of testing.

Test Procedure

The rapid macrocell test is a 15-week test. Corrosion rate and corrosion potential measurements are taken daily for the first week and weekly thereafter. The exposed area of the anode bar is used to calculate the corrosion rate, which is calculated based on the voltage drop measured across the 10 ohm resistor using Faraday's equation (equation 2 in Figure 10).

$$\text{Rate} = K \frac{V\ m}{n\ F\ D\ R\ A} \qquad \text{(eq. 2)}$$

Figure 10. Equation. Faraday's equation for corrosion rate based on measured voltage.

where the rate is given in µm/yr,

- K = conversion factor = $31.5 \cdot 10^4$ amp·µm sec/µA·cm·yr
- V = measured voltage drop across resistor, millivolts
- m = atomic weight of the metal (for iron, m = 55.8 g/mol)
- n = number of ion equivalents exchanged (for iron n = 2 equivalents)
- F = Faraday's constant = 96485 coulombs/equivalent
- D = density of the metal, g/cm^3 (for iron, D = 7.87 g/cm^3)
- R = resistance of resistor, ohms = 10 ohms for the test
- A = surface area of anode exposed to solution

In some cases, the corrosion rate may appear to be negative. This negative corrosion rate does not indicate negative corrosion. Rather, it is caused by minor differences in the oxidation rate between the single anode bar and cathode bars.

Determining the corrosion rate by taking voltage readings across the 10 ohm resistor (referred to as the macrocell corrosion rate) has the potential to miss localized corrosion, where the current flow between the anodic and cathodic reactions does not pass through the resistor placed between test bars. To capture both localized and general corrosion (referred to as the total corrosion rate), linear polarization resistance (LPR) tests are performed every three weeks. In addition, the corrosion potential is measured at both the anode and cathode using a silver-silver chloride electrode. Potential readings are converted to an equivalent copper-copper sulfate electrode for presentation. After 15 weeks, the bars are removed from testing, and the condition of the bars is photographed.

CHAPTER 3: DURABILITY TESTING—RESULTS AND DISCUSSION

Although classification tables based on susceptibility to chloride ion permeability are recommended in AASHTO T 358, the classification levels with respect to durability parameters may or may not be adequate. Of interest for concrete pavement performance, this study verifies the recommended CIP classification levels against actual durability testing such as corrosion, salt scaling, and freeze-thaw. Durability tests were conducted in parallel with electrical surface resistivity testing to compare performance classifications for each method. This chapter presents the results of the experimental study, followed by a discussion on the relationship between concrete electrical conductivity and durability performance parameters.

FREEZE-THAW DURABILITY

The action of freezing and thawing on a concrete material ultimately leads to the development of microcracking, altering the mechanical properties of the material, and physical degradation of a concrete element through loss of material. To evaluate the performance of a given concrete mixture, standard freeze-thaw testing can be performed. For this study, a series of mixtures were evaluated in accordance with procedure B defined in ASTM C666. The method is intended to evaluate the resistance to frost by measuring the change in resonant frequency of a specimen over the exposure regimen. As the mechanical properties of the material degrade, the resonant frequency measured will decay, as it is related to the dynamic modulus of elasticity of the material. For this study, the performance threshold is a maximal loss of 40% of the relative dynamic modulus. The results are presented by air-entrainment categories (non-air-entrained and air entrained), as air entrainment is assumed to be the prevailing factor to achieve adequate frost resistance.

Non-Air-Entrained Concrete Mixtures

As demonstrated in Figures 11 to 14, none of the non-air-entrained mixtures satisfied freeze-thaw performance criteria established at a threshold of 60% of the relative dynamic modulus. Once the entire set of sample mixtures surpassed the threshold, testing was terminated.

The 40% reduction in relative dynamic modulus is seen by the 20th cycle for all mixtures, except for OPC mixtures with a 0.45 w/cm ratio and a 0.4 w/cm ratio, which failed by cycle 35 and 40, respectively. In this case, w/cm ratio seems to impact the performance of the mixture. Mixtures containing SCMs of lower w/cm ratio slightly improved in performance; however, the results are not significantly different. As expected, a quality air void system is required to achieve desirable performance levels.

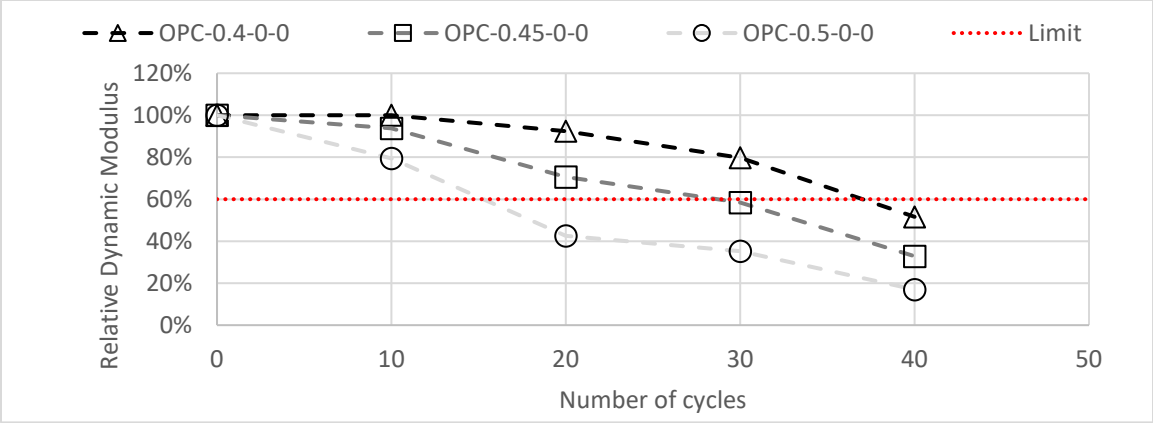

Figure 11. Graph. Relative dynamic modulus of elasticity versus number of freeze-thaw cycles for 0.4 w/cm, 0.45 w/cm, and 0.5 w/cm non-air-entrained ordinary Portland cement mixtures.

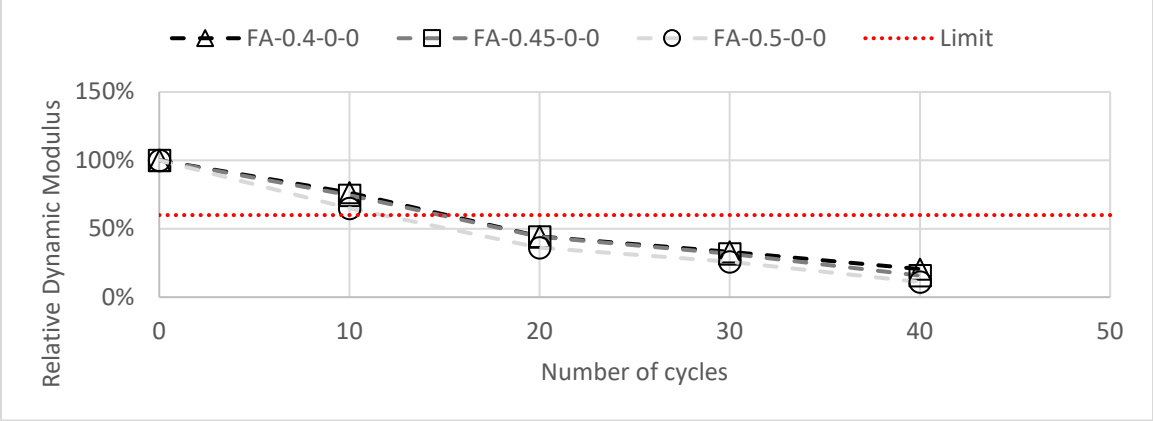

Figure 12. Graph. Relative dynamic modulus of elasticity versus number of freeze-thaw cycles for 0.4 w/cm, 0.45 w/cm, and 0.5 w/cm non-air-entrained fly ash mixtures.

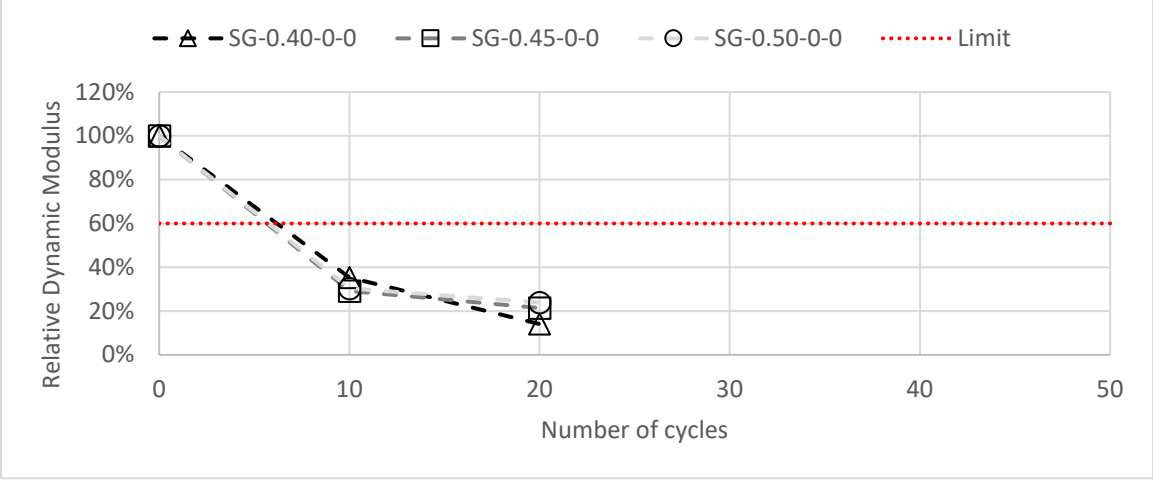

Figure 13. Graph. Relative dynamic modulus of elasticity versus number of freeze-thaw cycles for 0.4 w/cm, 0.45 w/cm, and 0.5 w/cm non-air-entrained slag mixtures.

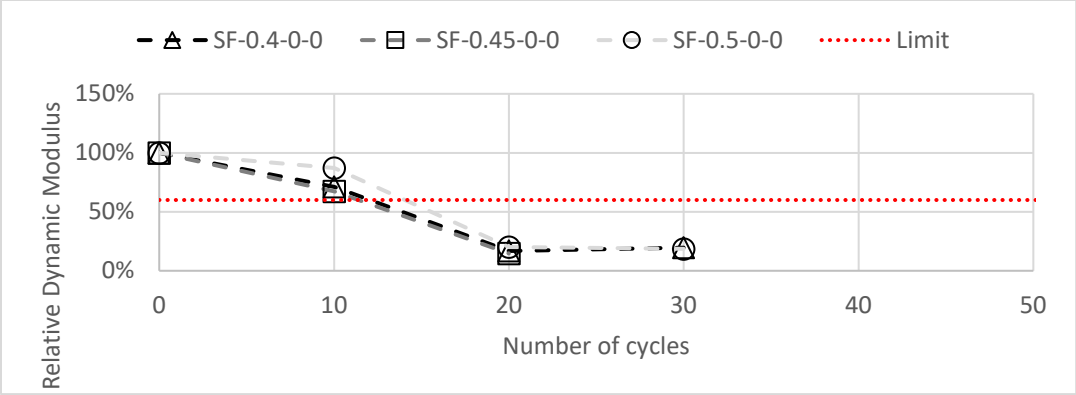

Figure 14. Graph. Relative dynamic modulus of elasticity versus number of freeze-thaw cycles for 0.4 w/cm, 0.45 w/cm, and 0.5 w/cm non-air-entrained silica fume mixtures.

Air-Entrained Concrete Mixtures

For air-entrained mixtures, all mixtures satisfied the performance criteria. The presence of air ranging between 5% and 7% for the evaluated mixtures provided an adequate defense against frost. For OPC mixtures (Figure 15), a relative dynamic modulus of 88.9%, 81.5%, and 74.3% was achieved for the 0.4 w/cm, 0.45 w/cm, and 0.5 w/cm concrete samples, respectively. Approaching the 300th cycle, a change in degradation rate is noticeable, potentially indicating damage progression toward failure. The 0.5 w/cm sample visually exhibited a slight loss of material at the surface of the prism. Nonetheless, OPC mixtures still performed adequately.

Mixtures containing SCMs performed best with an approximate 2% to 10% loss in relative dynamic modulus (Figures 16 to 18). Again, w/cm ratio had a minor impact on the performance of the material. As seen for the OPC mixtures, a lower w/cm ratio (i.e., 0.4 w/cm ratio) leads to an increase in performance. Concrete mixtures containing 40% slag cement replacement and 8% silica fume performed best. There is a slight degradation in the relative dynamic modulus for fly ash mixtures of lower w/cm ratio. Still, none of the samples exhibited visual signs of physical degradation at the end of the cyclic exposure.

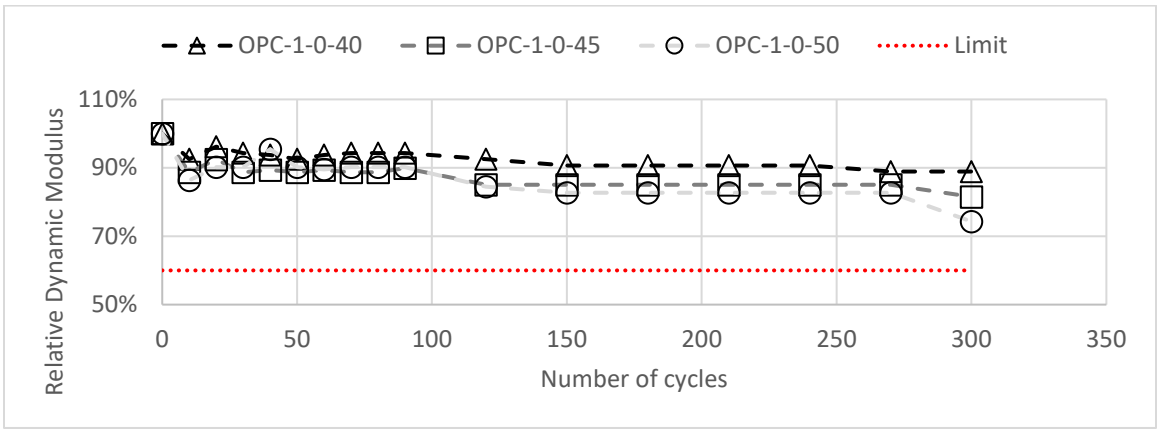

Figure 15. Graph. Relative dynamic modulus of elasticity versus number of freeze-thaw cycles for 0.4 w/cm, 0.45 w/cm, and 0.5 w/cm air-entrained ordinary Portland cement mixtures.

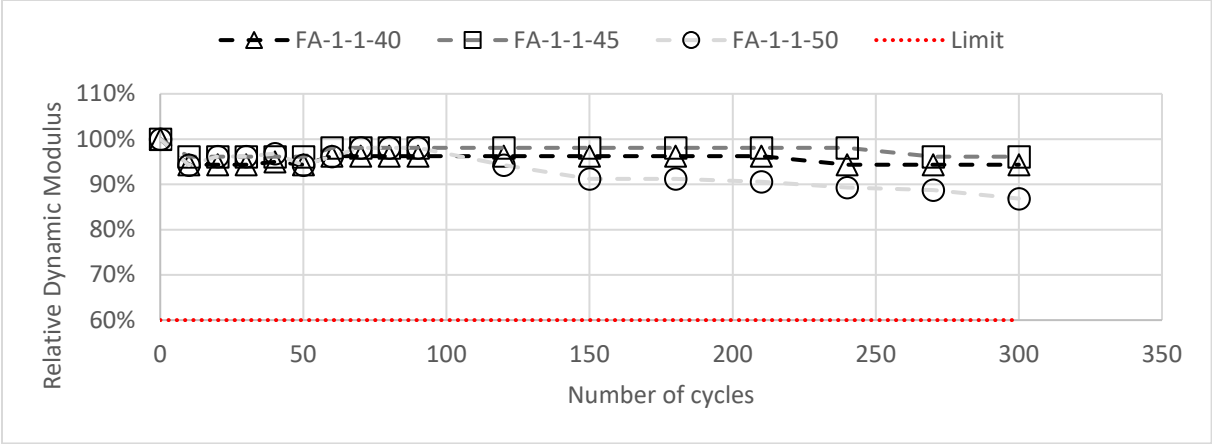

Figure 16. Graph. Relative dynamic modulus of elasticity versus number of freeze-thaw cycles for 0.4 w/cm, 0.45 w/cm, and 0.5 w/cm air-entrained fly ash mixtures.

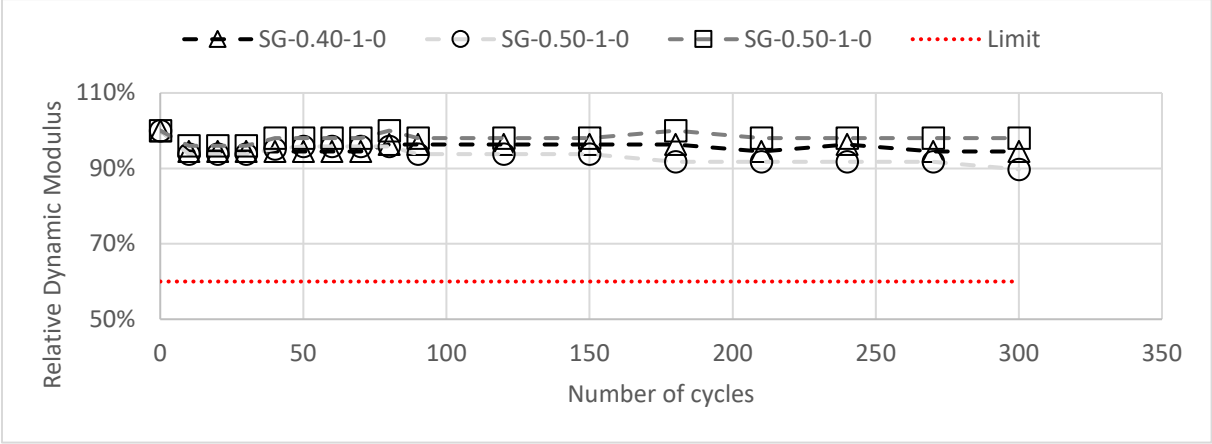

Figure 17. Graph. Relative dynamic modulus of elasticity versus number of freeze-thaw cycles for 0.4 w/cm, 0.45 w/cm, and 0.5 w/cm air-entrained slag mixtures.

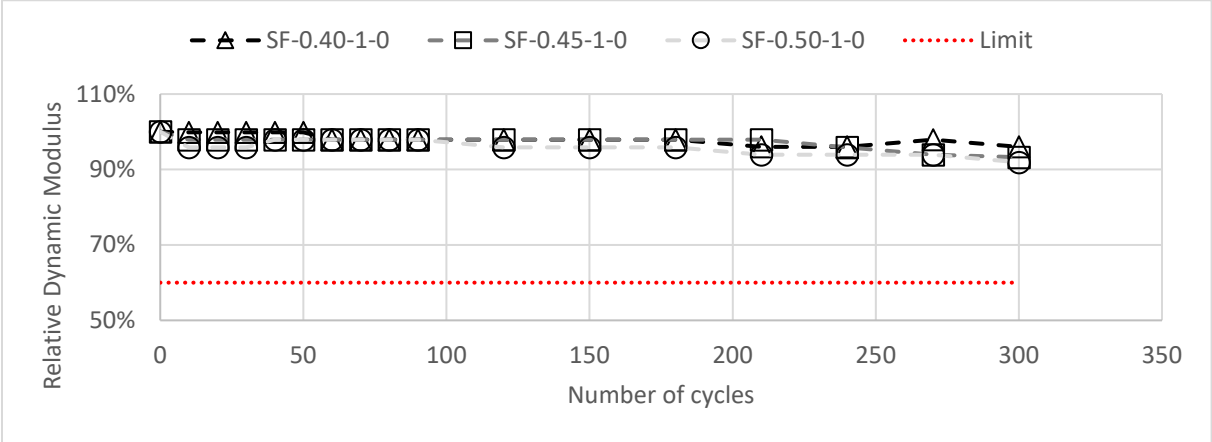

Figure 18. Graph. Relative dynamic modulus of elasticity versus number of freeze-thaw cycles for 0.4 w/cm, 0.45 w/cm, and 0.5 w/cm air-entrained silica fume mixtures.

SALT-SCALING DURABILITY

During winter months, the application of deicing salts on pavements is of importance for traffic safety. As the precipitation melts, salt in the brine solution is readily available at the concrete's surface. Under the action of freezing and thawing, the presence of the saline solution can lead to superficial physical damage of the concrete pavement. This surface scaling process is characterized by a gradual removal of flakes of mortar, small scales of concrete, or pop-out of coarse aggregate.

To evaluate the performance of a concrete mixture to salt scaling, several test methods have been recommended in literature. Research has demonstrated that the way the surface of the slab specimen is finished is of importance. Poor, over-finished, or inconsistent finishing practices may lead to premature failure of a sample. The pre-exposure conditioning practices and choice of ponding solution also affects the outcome of a test. Concrete containing SCMs are particularly sensitive to the latter due to latent development of the paste matrix (Hooton & Vassilev, 2012). For this study, a modified BNQ test method was followed. The performance threshold for the test was set at a cumulative weight loss in material of 0.5 kg/m^2 of slab surface, or 50 freeze-thaw cycles. The test was terminated once one of the thresholds was met. The results are presented by air-entrainment categories (non-air-entrained and air-entrained).

Non-Air-Entrained Concrete Mixtures

The susceptibility of non-air-entrained concrete mixtures to scaling in the presence of a salt solution was evaluated. The results are presented in Figures 20 through 22. Comparable to the results obtained for freezing and thawing testing, mixtures without air entrainment do not seem to perform adequately in terms of salt-scaling durability, with a few exceptions.

Starting with the OPC mixtures, a lower water-to-cement ratio is beneficial for scaling resistance. The OPC mixture with a 0.40 w/cm ratio satisfied the performance criteria after 50 cycles. Both specimens demonstrated localized scaling around a few coarse aggregates after 50 temperature cycles (Figure 19). A similar damage progression is seen for specimens with a 0.45 w/cm ratio and a 0.50 w/cm ratio, but at a greater scaling rate. Mixtures with a 0.45 w/cm ratio and a 0.5 w/cm ratio failed the test after 25 and 15 cycles, respectively. Both mixtures presented areas of extensive surface scaling with visible coarse aggregates.

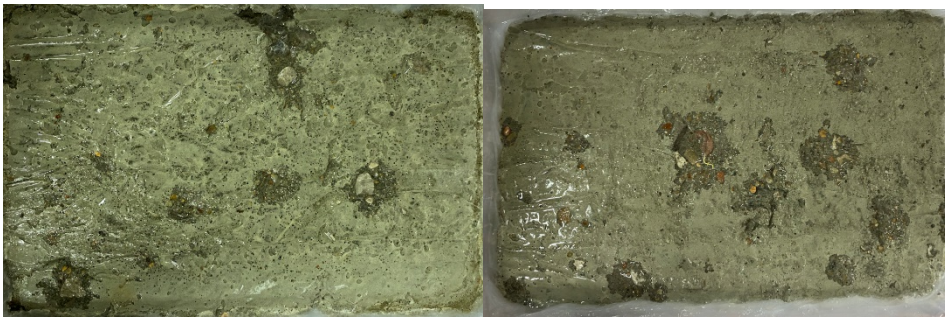

(a) (b)

Figure 19. Photo. Visual surface degradation after 50 cycles for OPC 0.40 w/cm ratio, non-air-entrained: (a) sample 1 and (b) sample 2.

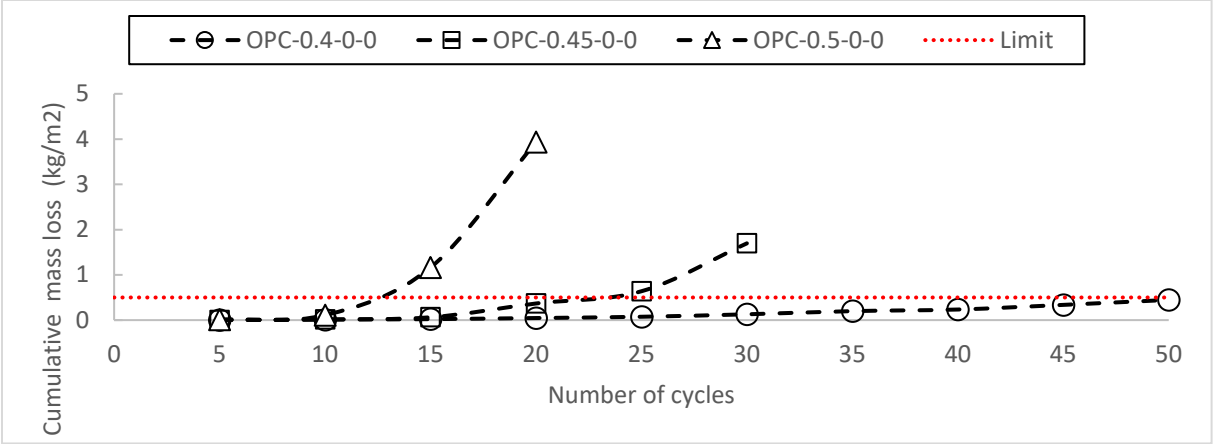

Figure 20. Graph. Relative cumulative mass loss versus number of freeze-thaw cycles for 0.4 w/cm, 0.45 w/cm, and 0.5 w/cm non-air-entrained ordinary Portland cement mixtures.

The effects of SCMs on salt-scaling performance were noticeable for the fly ash and silica fume samples. Unfortunately, there is no data available for the slag sample. Although the experiment was restarted twice, both trials resulted in nonconfidence in the results. The first trial was for an error in material source, and the second trial was due to chamber failure during time of exposure. The addition of fly ash had the most negative impact on concrete performance. Surface scaling with the coarse aggregate exposed is visible for most of the surface area for samples with a 0.45 w/cm ratio and a 0.5 w/cm ratio. In contrast, the sample with a 0.4 w/cm ratio demonstrated minimal damage. Visible scaling initiated after 20 cycles for the 0.4 w/cm leading to failure to meet the maximal performance criteria. For all three mixtures, once damage initiated, the rate in loss of material is substantial in comparison to silica fume.

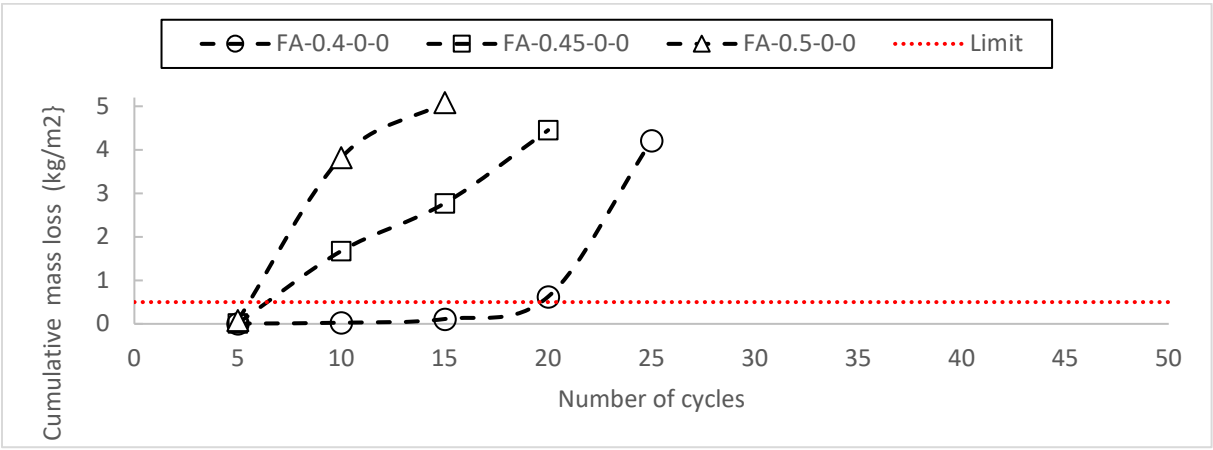

Figure 21. Graph. Relative cumulative mass loss versus number of freeze-thaw cycles for 0.4 w/cm, 0.45 w/cm, and 0.5 w/cm non-air-entrained fly ash mixtures.

The concrete samples with 8% silica fume replacement demonstrated a similar pattern to that of fly ash. The mixtures with a 0.45 w/cm ratio and a 0.5 w/cm ratio failed the test after 10 cycles, and the mixture with a 0.4 w/cm ratio quickly followed. However, the damage progression rate is lower than

that observed for the fly ash mixtures. Although surface scaling was visible across the surface of the slab specimens, the loose material that can be characterized has smaller and thinner mortar flakes.

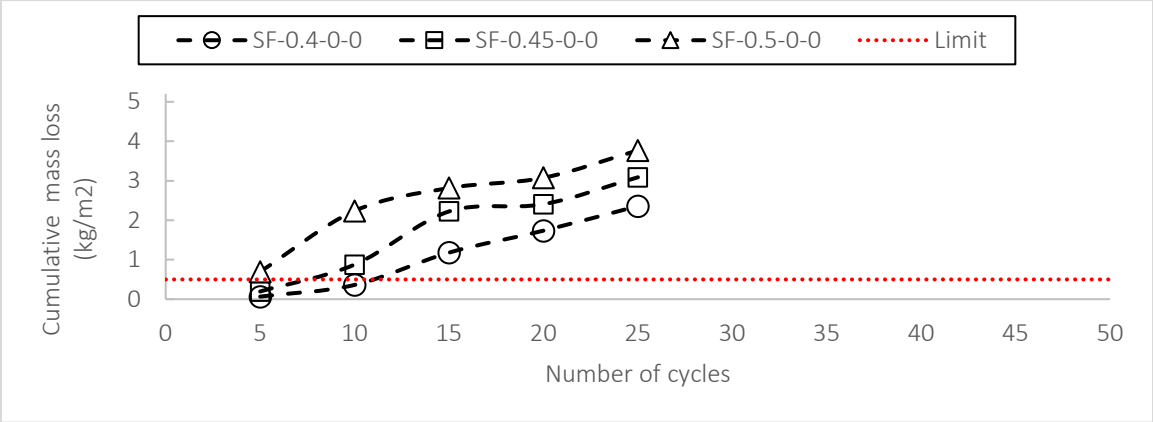

Figure 22. Graph. Relative cumulative mass loss versus number of freeze-thaw cycles for 0.4 w/cm, 0.45 w/cm, and 0.5 w/cm non-air-entrained silica fume mixtures.

Air-Entrained Concrete Mixtures

The material demonstrating the best performance to salt-scaling resistance is the OPC mixtures containing air entrainment (Figure 24). All three w/cm ratios behaved adequately, demonstrating minimal mass lost at the end of the 50 cycles. There were no visible coarse aggregates on the surfaces and no signs of aggregate pop-outs. Only localized scaling initiation was observed (Figure 23). Again, as determined previously, concrete freeze-thaw performance increased with the addition of air entrainment and lower w/cm ratio.

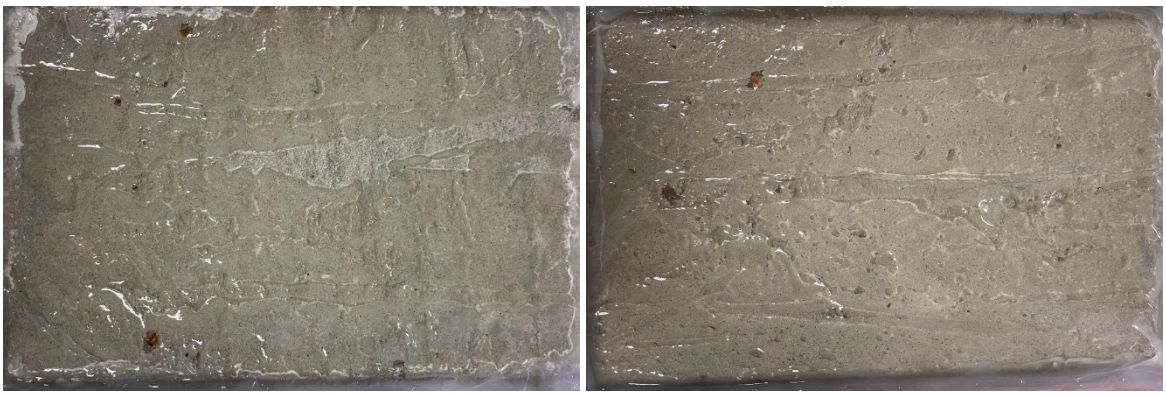

(a) (b)

Figure 23. Photo. Visual surface degradation after 50 cycles for OPC 0.40 w/cm ratio, air entrained: (a) sample 1 and (b) sample 2.

Although beneficial for freeze-thaw resistance, the use of SCMs in a concrete mixture does seem to affect scaling resistance in the presence of a salt solution (Figures 25 to 27). The results demonstrate the importance of maintaining a low w/cm ratio when using SCMs, as all samples with a 0.4 w/cm

ratio presented adequate performance. It also appears that the addition of air entrainment was beneficial for mixtures containing SCMs. Although there are visible signs of mortar flaking of the finished skin, the exposed surface does not seem to be affected as that previously seen for the non-air-entrained counterparts. The degradation progression is slow. A similar pattern is seen for the other two w/cm ratios, but damage progression varied per specimen. Surface scaling was minimal and present sparingly across the surface of the specimens. As previously mentioned, lost material was fine, except for a few instances of larger scales atop a large aggregate. The latter surface scaling type was noticeable mainly for mixtures with a 0.5 w/cm ratio. In comparison to non-air-entrained mixtures, the magnitude in loss in material is tenfold. Figure 28 presents an example comparison in degradation between two fly ash mixtures with a 0.5 w/cm ratio after 20 cycles.

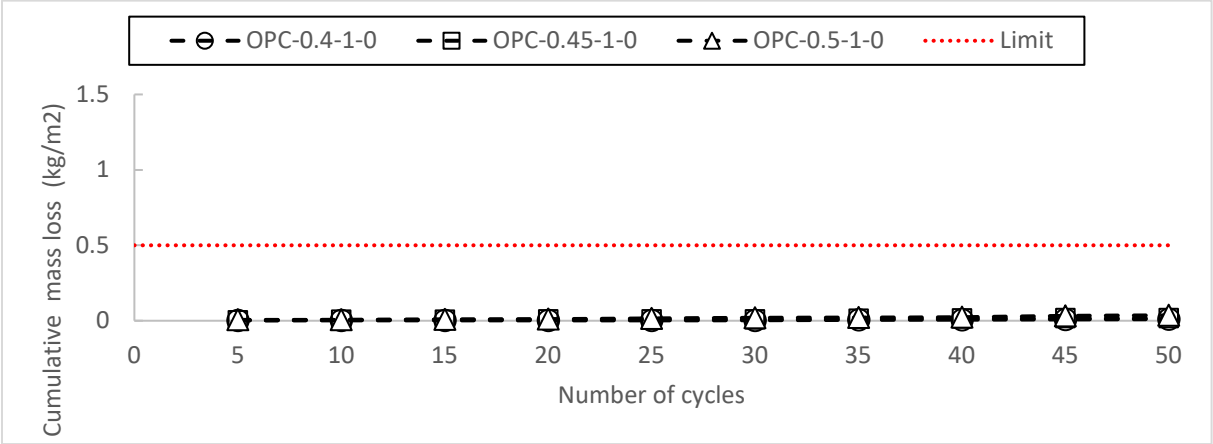

Figure 24. Graph. Relative cumulative mass loss versus number of freeze-thaw cycles for 0.4 w/cm, 0.45 w/cm, and 0.5 w/cm air-entrained ordinary Portland cement mixtures.

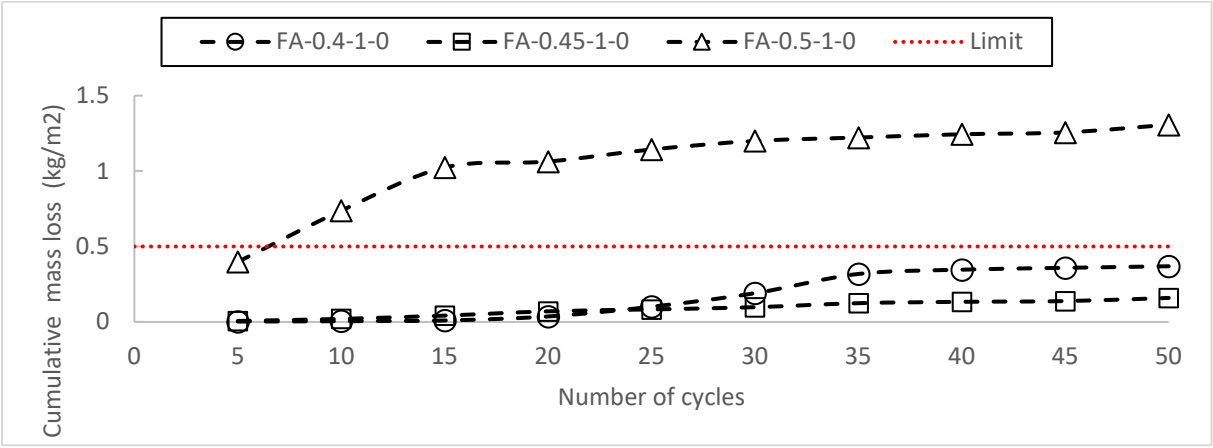

Figure 25. Graph. Relative cumulative mass loss versus number of freeze-thaw cycles for 0.4 w/cm, 0.45 w/cm, and 0.5 w/cm air-entrained fly ash mixtures.

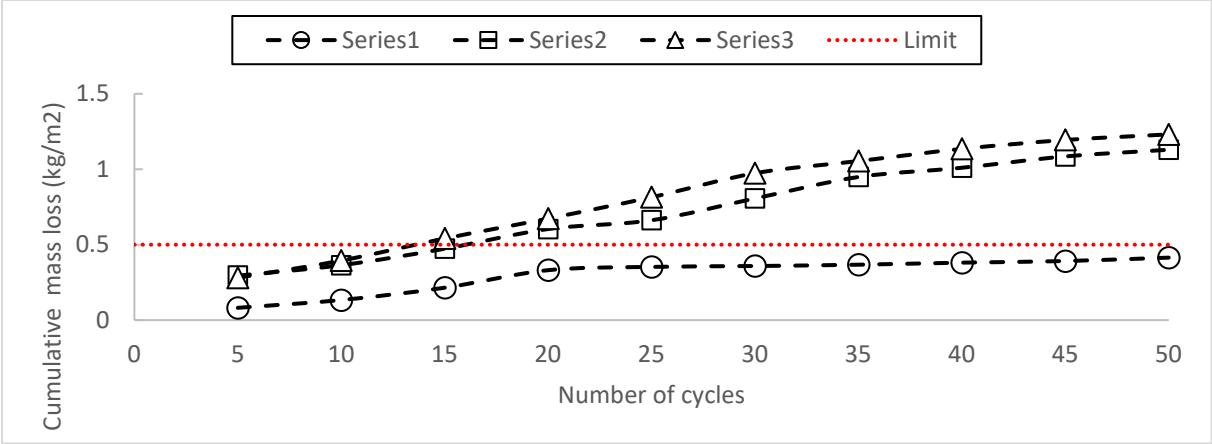

Figure 26. Graph. Relative cumulative mass loss versus number of freeze-thaw cycles for 0.4 w/cm, 0.45 w/cm, and 0.5 w/cm air-entrained slag mixtures.

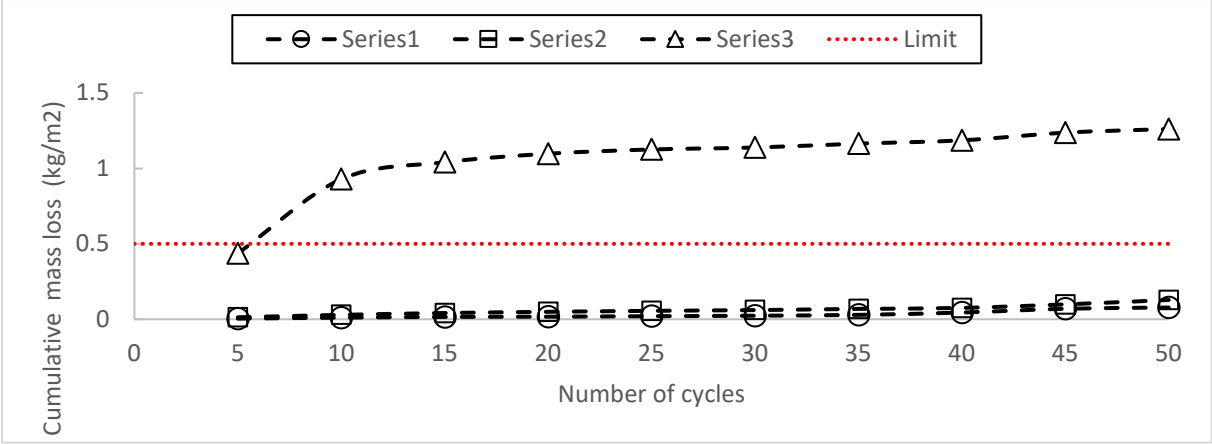

Figure 27. Graph. Relative cumulative mass loss versus number of freeze-thaw cycles for 0.4 w/cm, 0.45 w/cm, and 0.5 w/cm air-entrained silica fume mixtures.

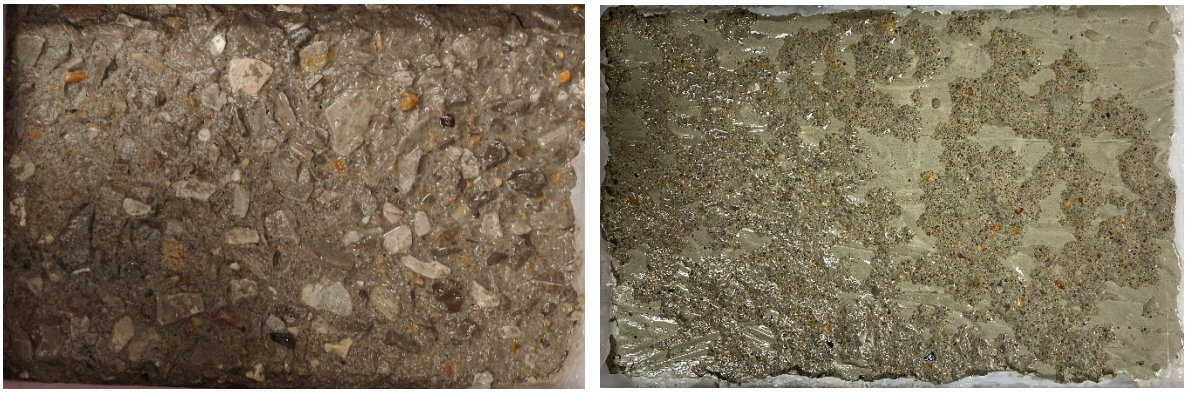

(a) (b)

Figure 28. Photo. Degradation comparison after 20 cycles between two 0.5 w/cm concrete mixtures containing fly ash: (a) without air and (b) with air entrainment.

CORROSION DURABILITY

Chloride ions are an aggressive agent that affects the durability of a reinforced concrete structure. They can pass through concrete cover and lead to the corrosion of embedded steel. Corrosion can be seen as an oxidation process involving the conversion of steel into its more chemically stable forms, such as ferric hydroxide, due to an electrochemical reaction with their ambient environment. For this study, corrosion assessment was performed following the rapid macrocell test outlined in the Annex of ASTM A955. Mixture design parameters such as w/cm ratio and presence of SCMs influencing the mixtures' potential to ionic ingress and corrosion initiation are evaluated through the macrocell corrosion rate.

Macrocell Corrosion Rate

Figures 29 through 31 present the average macrocell corrosion rates for specimens with 100% Portland cement, 20% fly ash, 40% slag, and 8% silica fume, respectively. As demonstrated in the figures, corrosion rates generally increased as w/cm ratio increased. Corrosion rates were generally unaffected by the addition of a SCM or air-entraining admixture, suggesting w/cm ratio is the dominating factor in this test. This may be due to the SCMs not fully hydrating during the relatively short curing period (7 days wet curing, 21 days dry curing). Although all specimens exhibited trends of decreasing corrosion rates as the test continued, the specimens with SCMs saw greater reductions in corrosion rate at later ages than specimens with 100% Portland cement, supporting this theory.

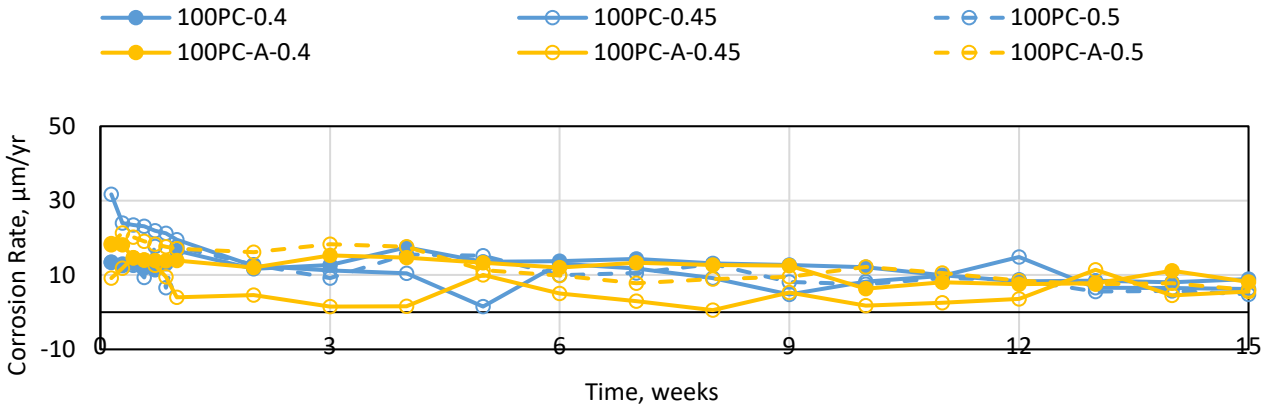

Figure 29. Graph. Macrocell corrosion rate for 100% PC specimens.

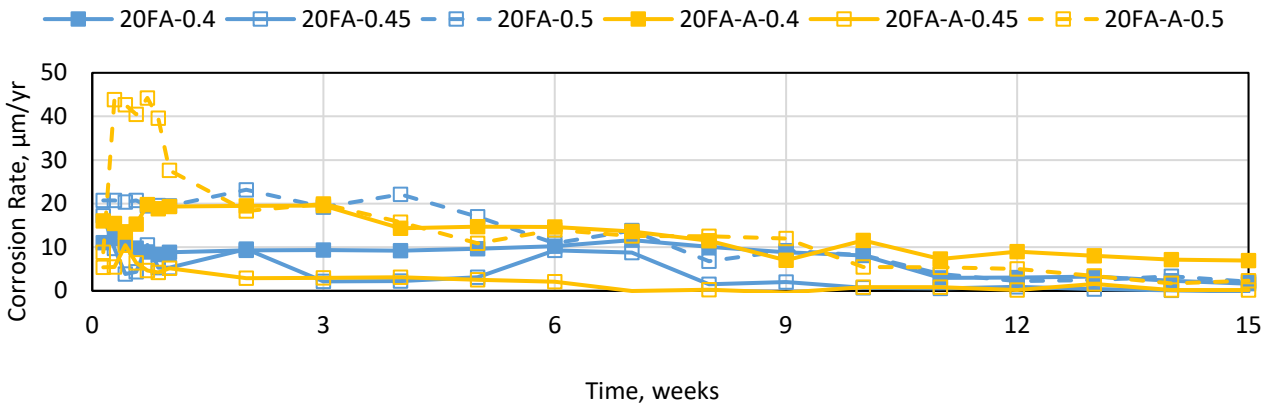

Figure 30. Graph. Macrocell corrosion rate for specimens with a 20% replacement with fly ash.

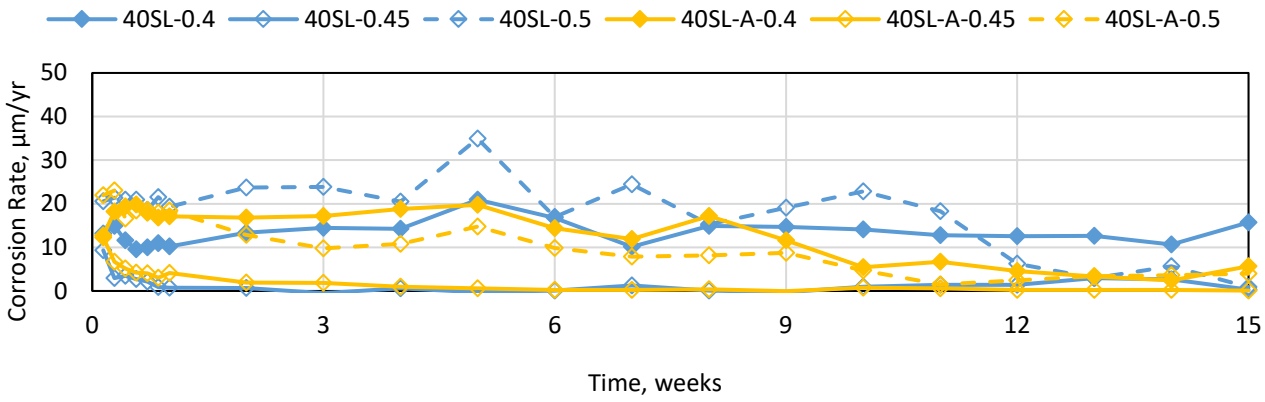

Figure 31. Graph. Macrocell corrosion rate for specimens with a 40% replacement with slag.

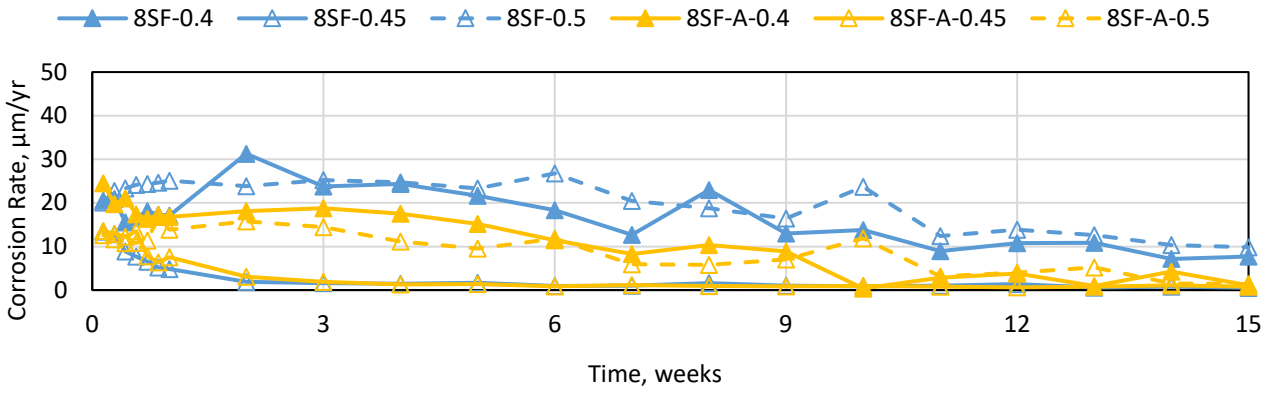

Figure 32. Graph. Macrocell corrosion rate for specimens with an 8% replacement with silica fume.

Average Total Corrosion Rate

Figures 33 through 36 present the average total (LPR) corrosion rates for the specimens with 100% Portland cement, 20% fly ash, 40% slag, and 8% silica fume, respectively. The trends generally match those seen in the macrocell corrosion rates, with w/cm ratio being the dominating factor in determining corrosion rate. Both OPC mixtures with a 0.4 w/cm ratio performed well with a low LPR at the end of the test period; however, overall trends are similar for all mixture types. The reduction in corrosion rate over time that was observed in macrocell corrosion rates is not seen in total corrosion rates. This indicates a shift from uniform to localized corrosion at later ages in the test.

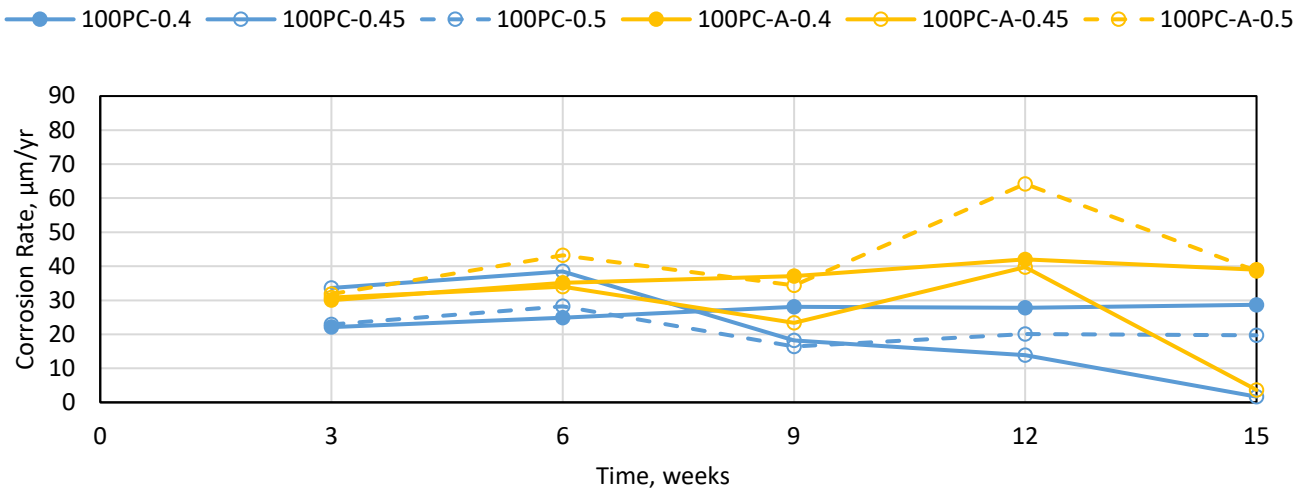

Figure 33. Graph. Total corrosion rate for 100% PC specimens.

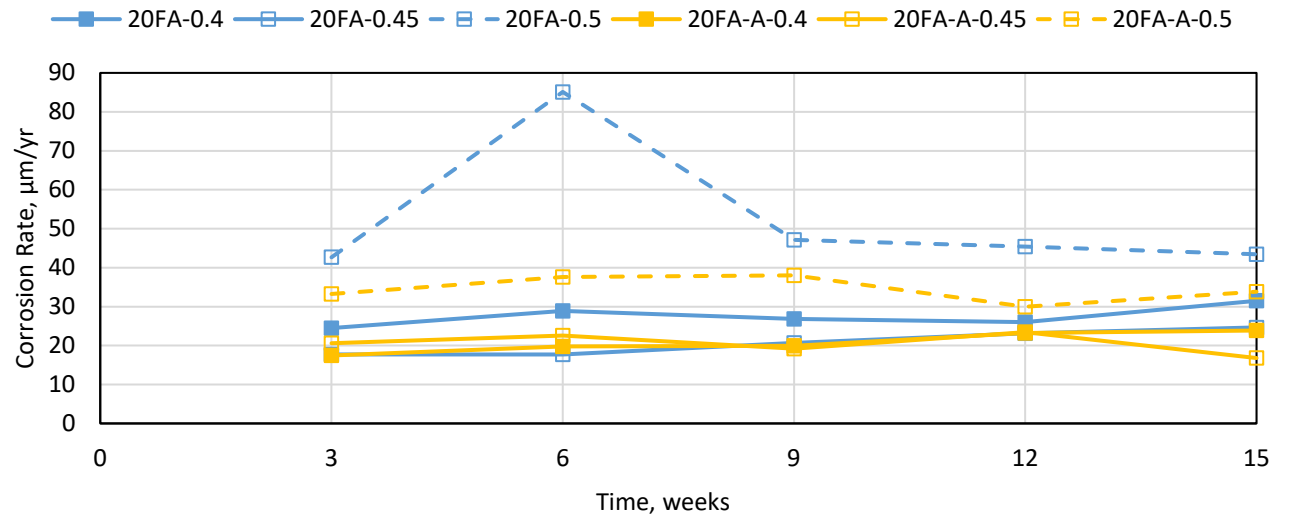

Figure 34. Graph. Total corrosion rate for specimens with a 20% replacement with fly ash.

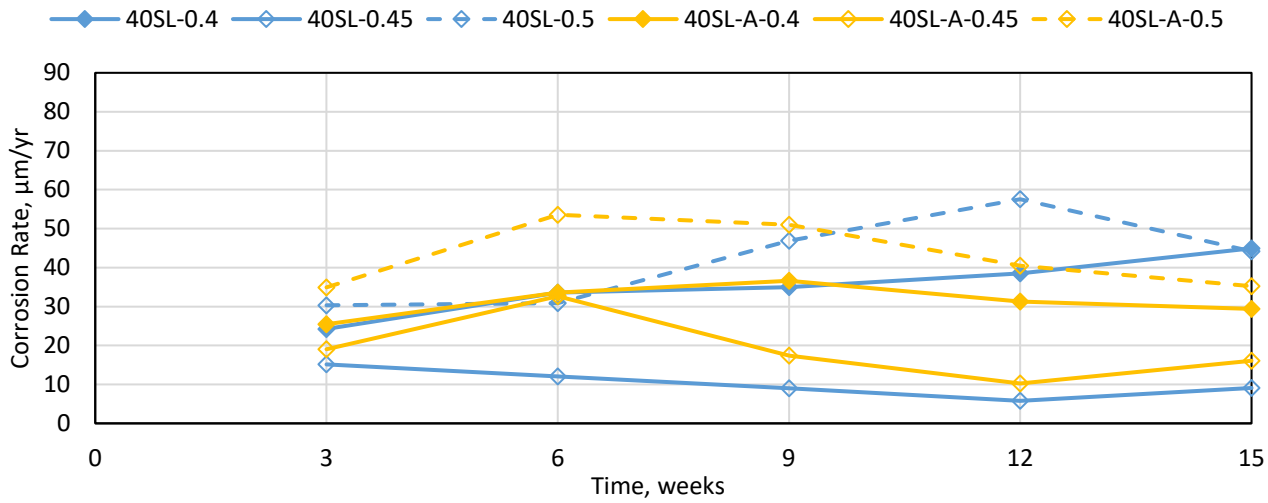

Figure 35. Graph. Total corrosion rate for specimens with a 40% replacement with slag.

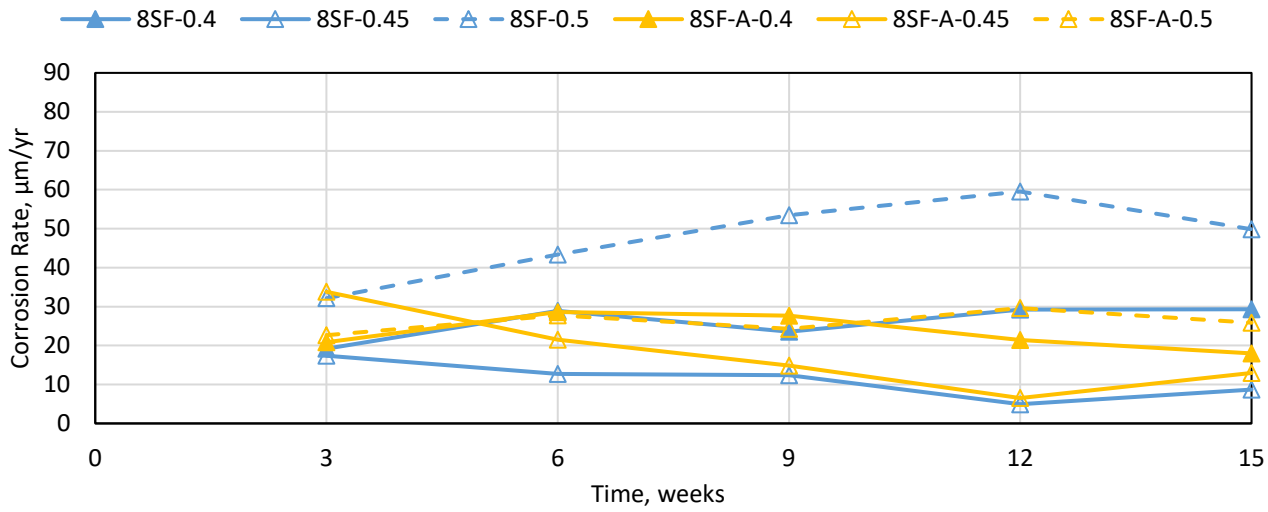

Figure 36. Graph. Total corrosion rate for specimens with an 8% replacement with silica fume.

Visual Signs of Corrosion

Figure 37 presents the anode bars from specimens with 100% Portland cement, 20% fly ash, 40% slag, and 8% silica fume, respectively, after 15 weeks of testing. The photographs are of specimens with a 0.4 w/cm ratio. Similar observations were made on specimens with higher w/cm ratios. Several anode bars from specimens exhibited signs of staining or cracking after 15 weeks of testing. No corrosion products were visible on the cathode bars. (The cathode bar photographs are not displayed.)

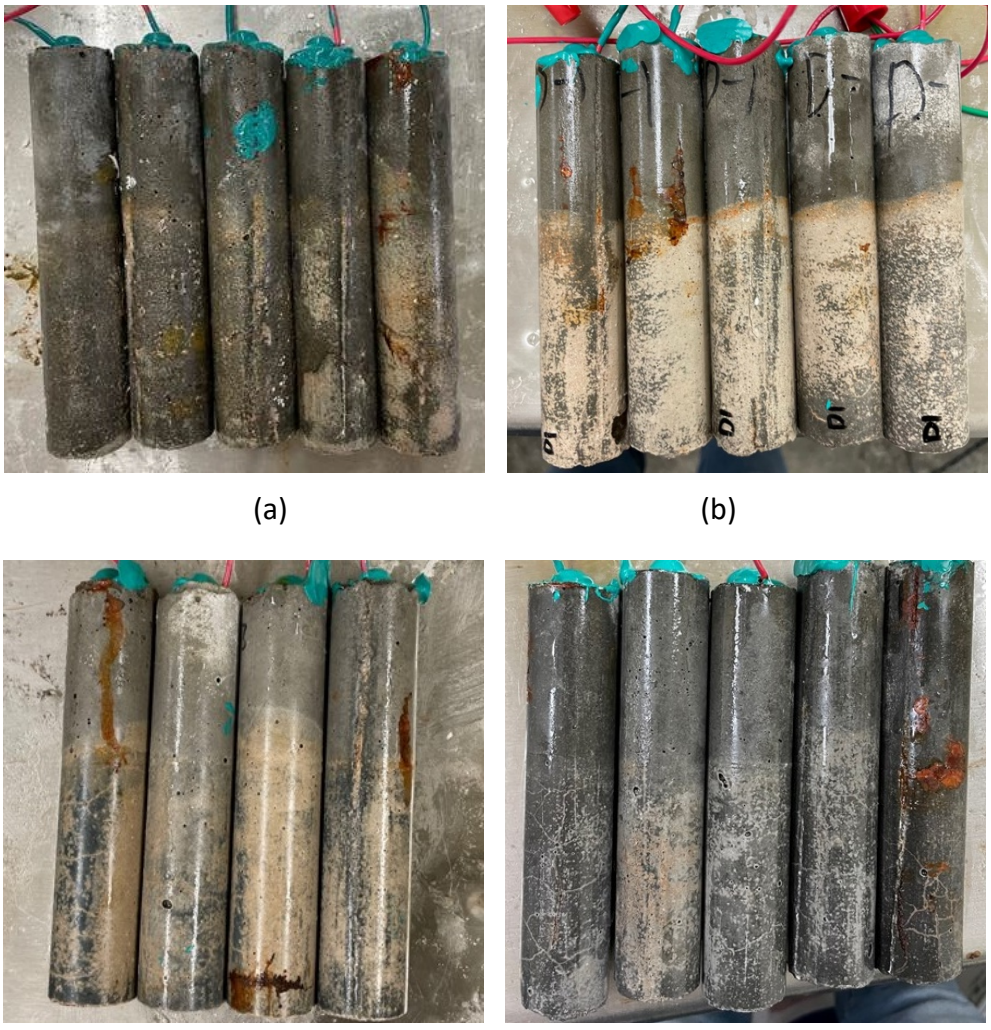

(a) (b)

(c) (d)

Figure 37. Photo. Anode bars with a 0.4 w/cm ratio after 15 weeks of testing: (a) OPC, (b) fly ash, (c) slag, and (d) silica fume.

Resistivity Testing

Electrical surface resistivity was conducted on companion specimens while conducting durability testing. The results for the series of samples are presented in Figures 38 through 45. The results are also presented in Appendix A, where a comparative view of all mixtures on a single graph is provided. The results demonstrate that the resistivity of a material changes with w/cm ratio and SCM content. Here, the addition of an air-entraining admixture did not have a significant influence on the resistivity measurement.

OPC mixtures recorded the lowest values, while silica fume mixtures recorded substantially higher values. In terms of CIP classification, the OPC mixtures would classify as high CIP after 28 days of testing and would maintain this classification after 98 days of curing. Only mixtures with a 0.4 w/cm ratio barely surpass the moderate classification. Similarly for the fly ash mixtures, the initial 28-day

classification is deemed high CIP. However, the latent reactivity of the pozzolan is demonstrated by an increase in the rate of resistivity gain over time. Thus, the material achieves a moderate classification by day 56, which is maintained until day 98. The difference in resistivity between OPC and fly ash mixtures is marginal. The non-air-entrained OPC mixtures recorded 56-day resistivity values of 12.0 kΩ-cm, 10.6 kΩ-cm, and 9.7 kΩ-cm for the mixtures with a 0.40 w/cm, 0.45 w/cm, and 0.5 w/cm ratio, respectively, and 14.5 kΩ-cm, 13.0 kΩ-cm, and 10.9 kΩ-cm for the fly ash mixtures.

The initial rate in resistivity gain for the slag and silica fume mixtures is substantially greater; thus, both mixtures achieve a low classification by day 28. This trend continues until day 56, permitting low to very low classifications. The greater gain in resistivity over time for the silica fume mixtures makes this mixture design substantially greater than slag. The non-air-entrained slag mixtures recorded 56-day resistivity values of 41.3 kΩ-cm, 36.1 kΩ-cm, and 37.5 kΩ-cm for the mixtures with a 0.40 w/cm, 0.45 w/cm, and 0.5 w/cm ratio, respectively. Meanwhile, the silica fume mixtures recorded 64.0 kΩ-cm, 50.2 kΩ-cm, and 46.5 kΩ-cm.

With a wide difference in resistivity value and classification, is an OPC mixture with a 0.4 w/cm ratio substantially less durable than a mixture with silica fume replacement? Under such classification, an OPC mixture demonstrating adequate durability performance may be disqualified. Or, a mixture of high w/cm ratio containing SCMs such as silica fume may provide a “boost” in resistivity to meet the minimal CIP classification.

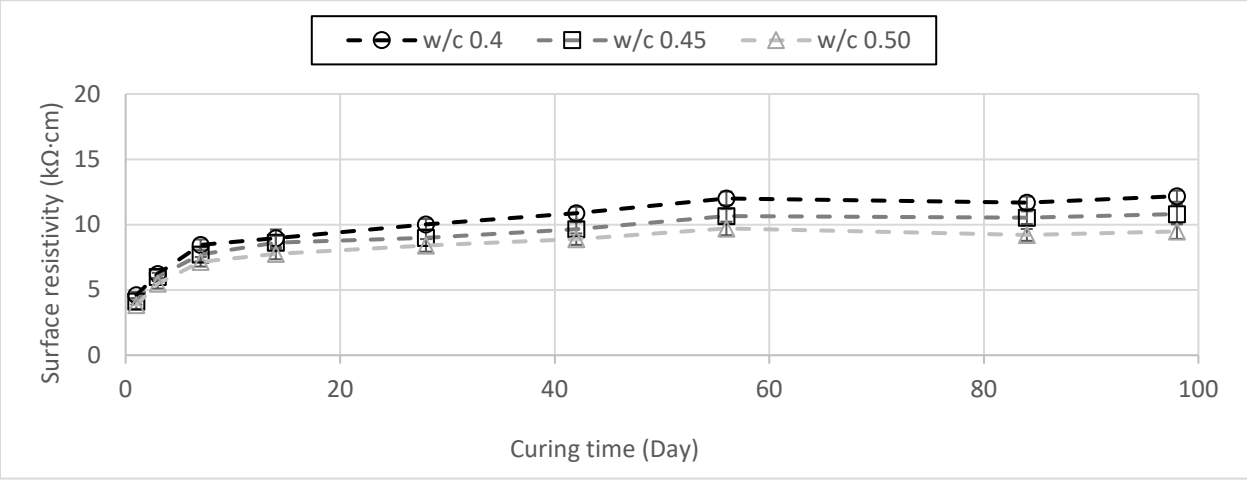

Figure 38. Graph. Gain in surface resistivity over time for 0.4 w/cm, 0.45 w/cm, and 0.5 w/cm ratio non-air-entrained OPC mixtures.

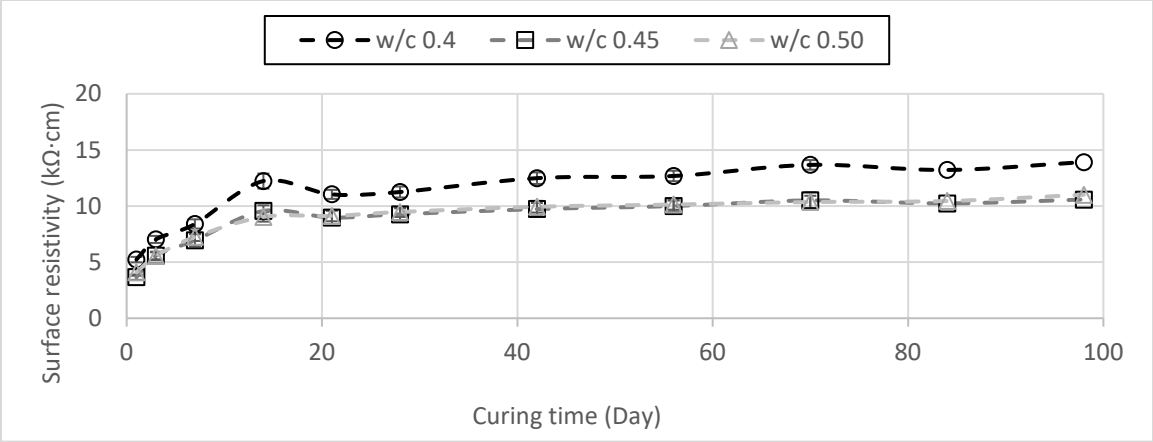

Figure 39. Graph. Gain in surface resistivity over time for 0.4 w/cm, 0.45 w/cm, and 0.5 w/cm ratio air-entrained OPC mixtures.

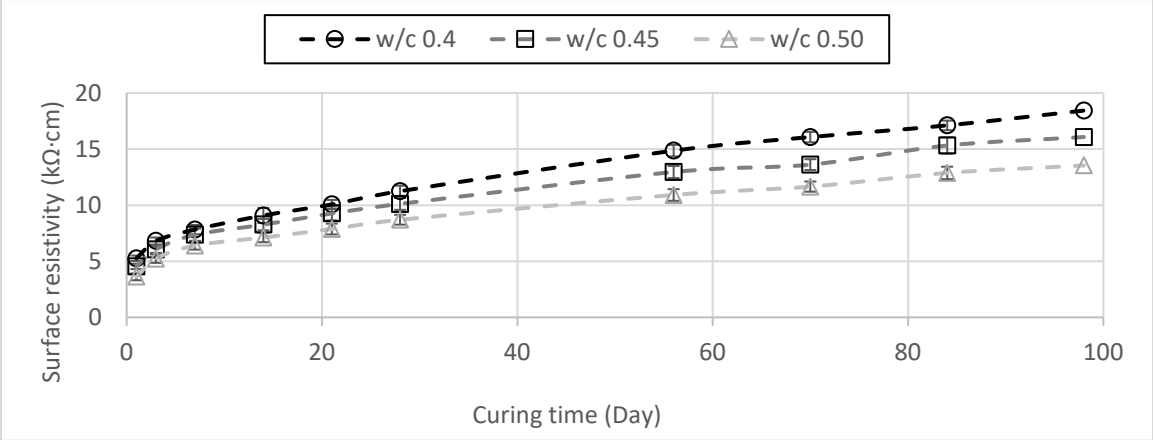

Figure 40. Graph. Gain in surface resistivity over time for 0.4 w/cm, 0.45 w/cm, and 0.5 w/cm ratio non-air-entrained fly ash mixtures.

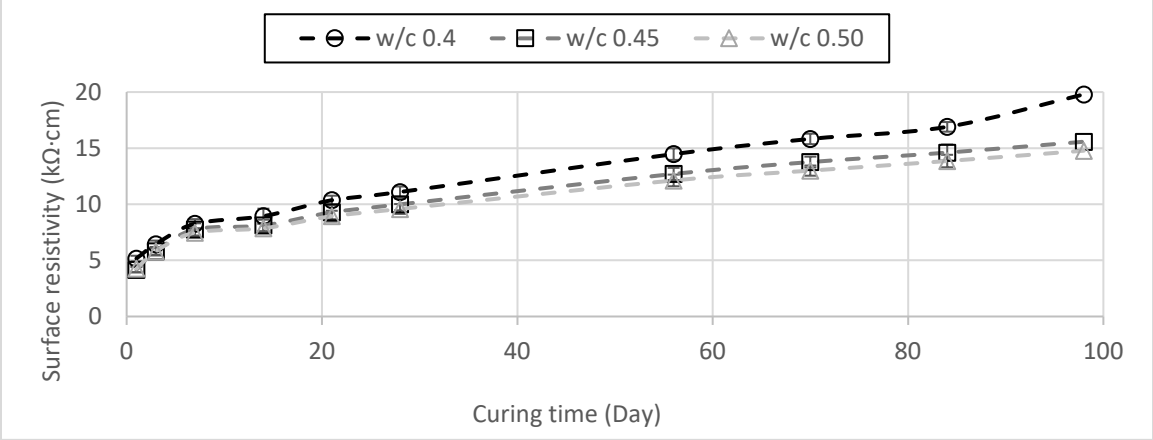

Figure 41. Graph. Gain in surface resistivity over time for 0.4 w/cm, 0.45 w/cm, and 0.5 w/cm ratio air-entrained fly ash mixtures.

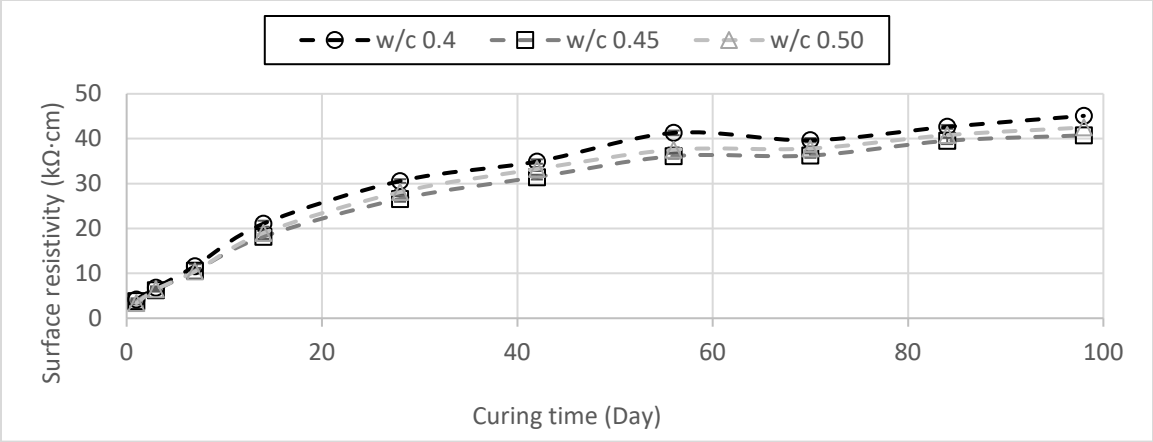

Figure 42. Graph. Gain in surface resistivity over time for 0.4 w/cm, 0.45 w/cm, and 0.5 w/cm ratio non-air-entrained slag mixtures.

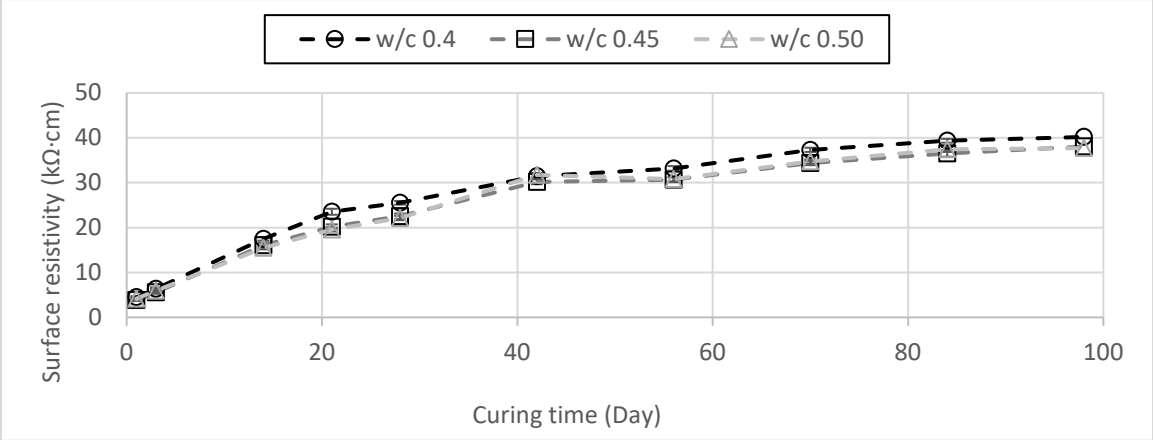

Figure 43. Graph. Gain in surface resistivity over time for 0.4 w/cm, 0.45 w/cm, and 0.5 w/cm ratio air-entrained slag mixtures.

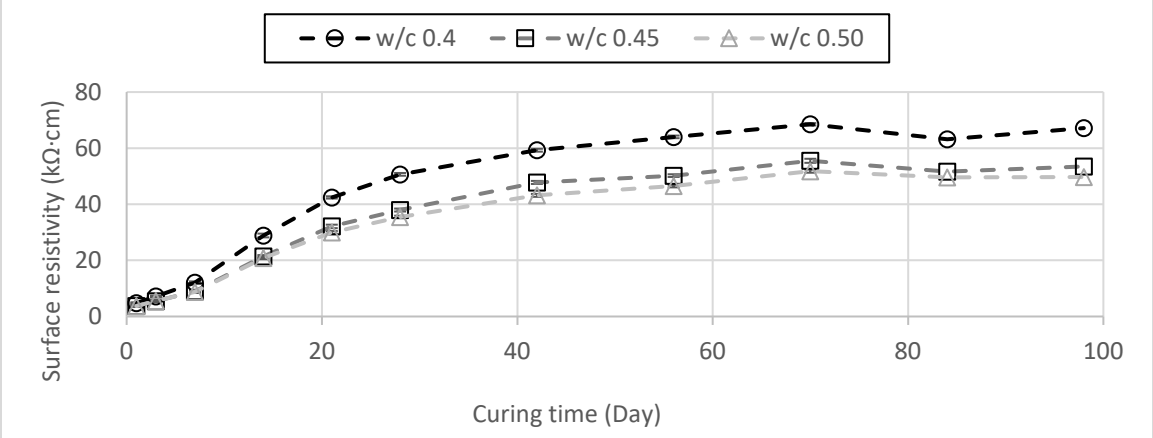

Figure 44. Graph. Gain in surface resistivity over time for 0.4 w/cm, 0.45 w/cm, and 0.5 w/cm ratio non-air-entrained silica fume mixtures.

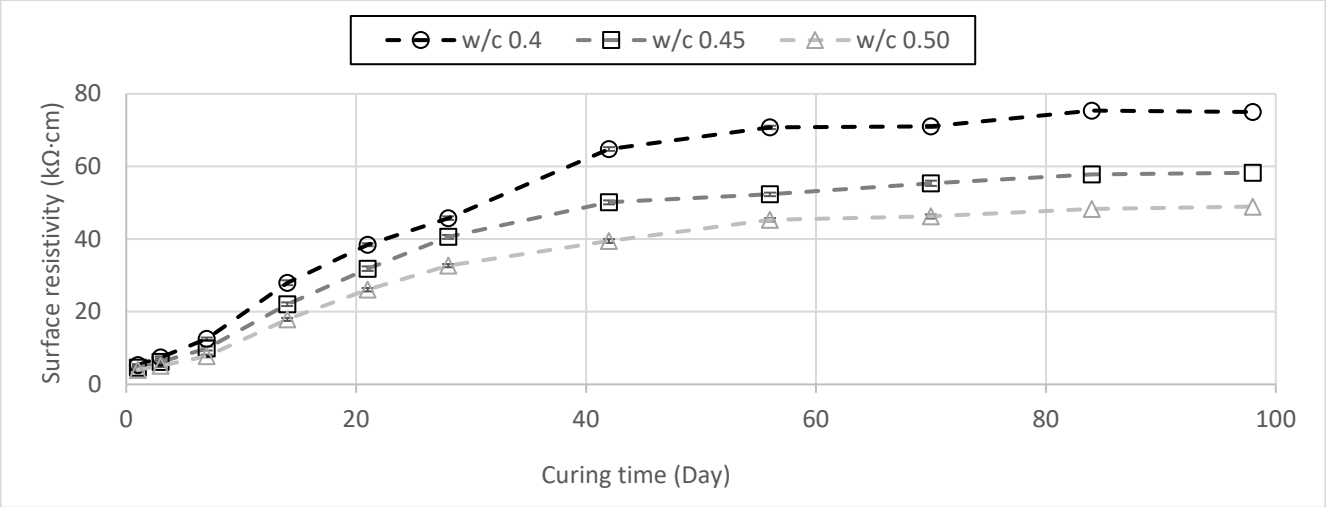

Figure 45. Graph. Gain in surface resistivity over time for 0.4 w/cm, 0.45 w/cm, and 0.5 w/cm ratio air-entrained silica fume mixtures.

COMPARISON BETWEEN DURABILITY PERFORMANCE AND ELECTRICIAL RESISTIVITY

The following sections provide a comparative analysis between surface resistivity and the results for durability testing.

Freeze-Thaw Durability

When concrete structures undergo freeze-thaw cycling, according to the hydraulic pressure model, ice is formed in the capillary pores of the hardened cement paste as temperature decreases. The associated volumetric increase will expel the excess water from the freezing sites toward the surrounding cement paste, causing hydraulic pressure (Power, 1945). The presence of a refined air void system can aid in relieving internal pressure by offering space for water to freeze. Freeze-thaw induced microcracks will develop in the cement paste capillaries once the pressure exceeds the tensile strength of the cement matrix (Coussy & Monteiro, 2008). Then, more water will be absorbed through these microcracks as the temperature rises. Therefore, subsequent cycles of freezing and thawing continue the expansion and will have a cumulative effect. This cumulative damage not only effects concrete properties, but also allows for further ingress of chlorides and other chemicals that can cause other durability issues (Wang et al., 2020). Based on the nature of the internal freeze-thaw damage mechanism, capillary absorption and permeation are the two leading sources of water penetration, and the freeze-thaw damage will initiate when the internal moisture content passes the critical degree of saturation (Li et al., 2012).

Thus, the prevention of water infiltration into the cementitious matrix as well as air entrainment are the best defenses against frost damage. The results of the study support the theory that there is a clear difference between air-entrained and non-air-entrained mixtures. However, when comparing the resistivity for both mixture types (Figure 46-A), there is no correlation, as the resistivity of a mixture is not affected by the presence of an admixture (Hartell, 2020).

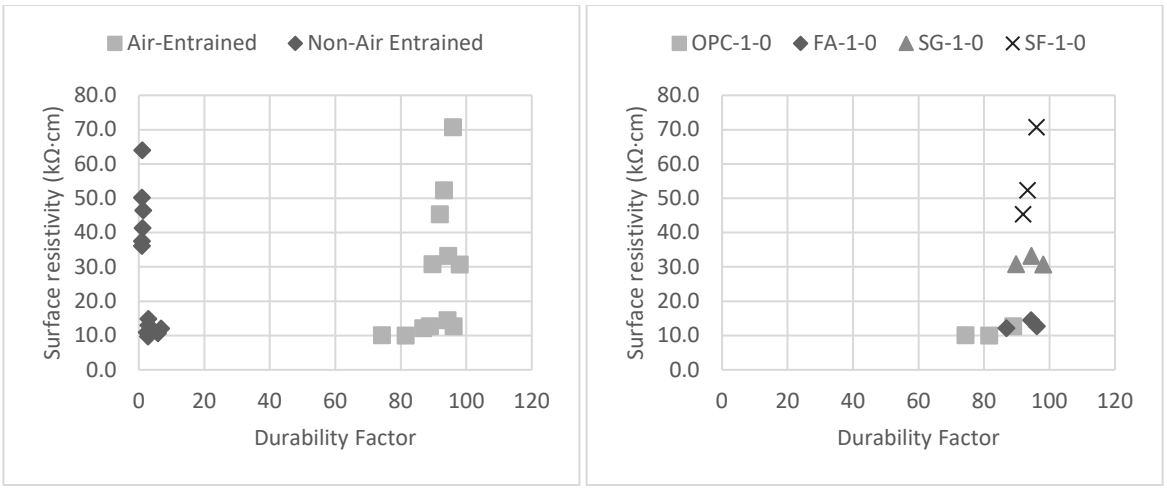

(a) (b)

Figure 46. Graph. 56-day surface resistivity versus durability factor: comparison between air-entrained and non-air-entrained mixtures and (b) mixtures of different SCMs.

When comparing the durability factor obtained for mixtures of varying SCM types (Figure 46-B), there is no existing relationship between resistivity and freeze-thaw performance. The silica fume mixtures, recording nearly double the value of that for slag mixtures and quadruple of that for fly ash mixtures, did not perform significantly better. After 56 days of curing, the fly ash mixtures barely met the moderate performance classification for chloride ion penetrability according to AASHTO T 358. In fact, the slag and silica fume mixtures met the low and very low criteria, respectively, and all three SCMs behaved similarly for freeze-thaw performance testing. Even the OPC mixture with a high ion chloride ion penetrability performed adequately. Therefore, resistivity does not seem to provide an indication of the frost performance of a mixture.

Salt-Scaling Durability

Salt scaling refers to the superficial damage induced by repeated freezing and thawing cycles of a saline solution on the surface of a cementitious body (Valenza & Sherer, 2006). The surface scaling process is characterized with a gradual removal of small chips, flakes of material, or pop-out of coarse aggregate in the worst-case scenario (Valenza & Sherer, 2007). The combination of mechanisms involved leading to the detrimental effects are complicated and still not well understood. In combination with frost damage, the glue spall mechanism was recently introduced as a major cause of salt scaling (Valenza & Sherer, 2006, 2007). According to the theory, ice and surface concrete are "glued" together in a composite form, as ice can penetrate the pores of concrete during freezing. The formation of ice will also increase the concentration of the remaining solution, which introduces brine pockets within the ice. The brine pockets are in liquid form, and, thus, are deemed to be a local weak zone on the surface of the ice. As temperature further decreases, the ice will tend to shrink more than the concrete as the mismatch of coefficient of expansion between them. Therefore, a crack on the ice will form due to the existing brine pockets and extend further down through the concrete, which eventually results in scaling of surface cementitious material. There is another possible detrimental chemical reaction involved in chloride-based salt-scaling deterioration. In this

process, the chlorides can react with a cement compound, forming calcium oxychloride with a general formula $3Ca(OH)_2 \cdot CaCl_2 \cdot nH_2O$ (Álava et al., 2016). The low temperature promotes the reaction, as oxychloride has relatively low solubility in this temperature range (Jones et al., 2020). The precipitation of calcium oxychloride occurs when the temperature is just above the freezing point. The ingress of solution may decrease, as this precipitation increases the paste tortuosity (Jones et al., 2020). The formation of calcium oxychloride crystals will induce expansion and deterioration and eventually cause surface scaling of concrete (Jones et al., 2020; Peterson et al., 2013). Therefore, the concrete's ability to resist solution and ionic penetration is of consequence when designing for salt-scaling durability.

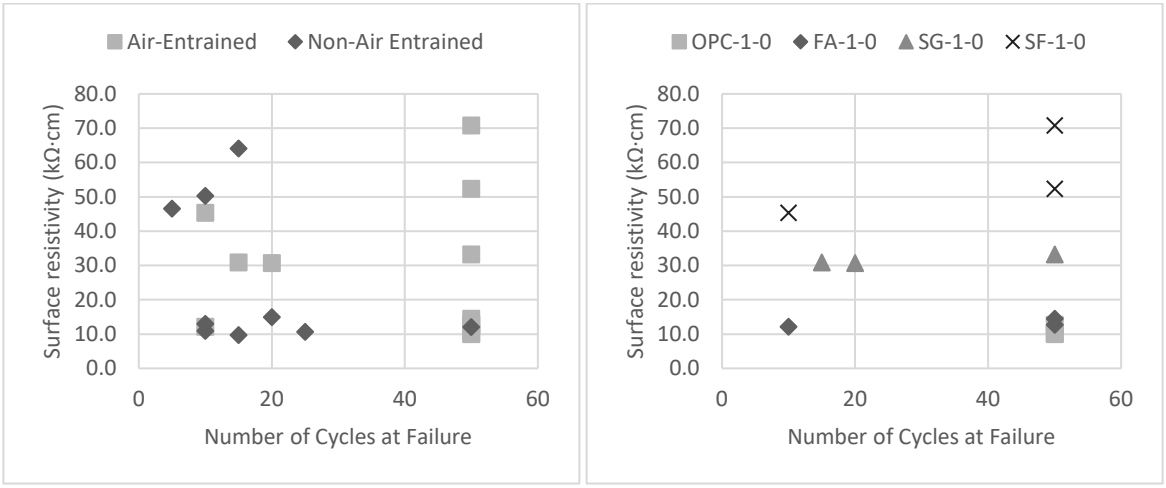

(a) (b)

Figure 47. Graph. Surface resistivity versus number of cycles at failure: comparison between (a) air-entrained and non-air-entrained mixtures and (b) mixtures of different SCMs.

As demonstrated in Figure 47, there is no existing relationship between resistivity and salt-scaling performance. In fact, the mixture design presenting the best scaling performance, OPC, recorded the lowest resistivity. Inversely, mixtures with higher resistivities do not necessarily perform well. In this case, the use of an SCM appears to be detrimental unless a low w/cm ratio is used. As previously mentioned, the presence of air entrainment seemed to be a contributing factor in increasing the performance of a concrete mixture (Figure 15 to 18). However, it was not the sole parameter, as mixtures containing both SMCs and air entrainment still demonstrated various levels of scaling. Therefore, resistivity does not seem to provide an indication of salt-scaling performance.

Corrosion Durability

Chloride ions are an aggressive agent that affects the durability of a reinforced concrete structure. They can pass through concrete cover and lead to the corrosion of embedded steel. Corrosion can be seen as an oxidation process involving the conversion of steel into its more chemically stable forms, such as ferric hydroxide, due to electrochemical reaction with their ambient environment. Concrete is alkaline in nature due to the presence of Ca(OH)2, NaOH, and KOH, which have a typical pH in the pore solution of concrete of 12.5–13.5 (Vollpracht et al., 2016). This high pH naturally passivizes the

reinforcing steel by creating an oxide film layer on the surface of the rebar, preventing further reactions on the surface. Chlorides that have reached this passive layer of the steel, in the presence of oxygen and water, destroy the layer and allow for corrosion to initiate (Montemor et al., 2003). Diffusion seems to have a dominant effect in the chloride ingression scenario, leading to corrosion of reinforcement within concrete (Khan et al., 2017; Stanish et al., 2001). Chloride ions enter concrete through the internal pores due to the concentration gradient between the external exposure surface and the pore solution of the cement matrix. Therefore, the chloride penetration rate highly depends on the physical properties of the pore structure of the cement matrix, which correlates with the water-to-cement ratio, curing condition, and age of the concrete, etc. (Song et al., 2008).

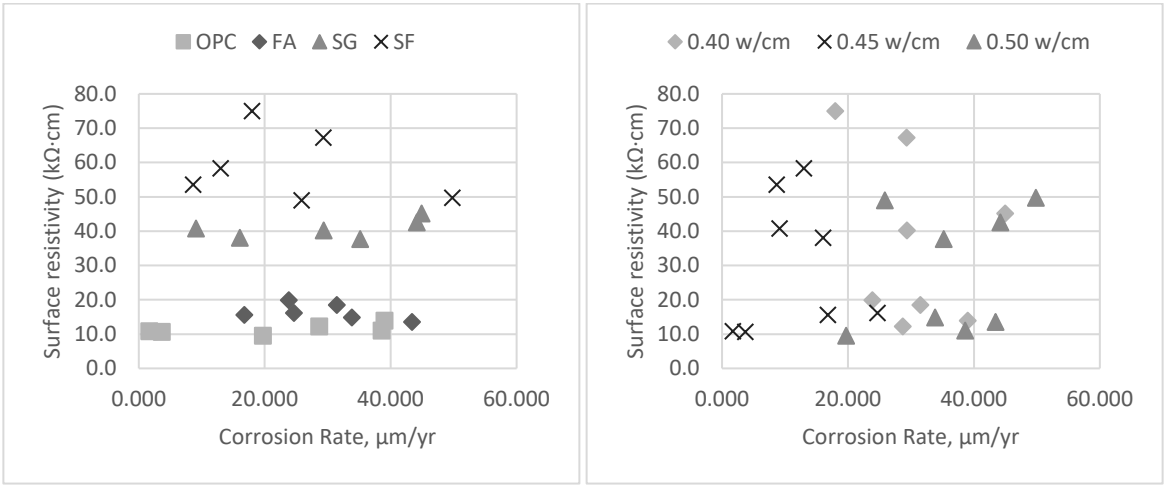

(a) (b)

Figure 48. Graph. Surface resistivity versus corrosion rate: (a) comparison between mixtures of different SCMs and (b) mixtures of varying w/cm ratios.

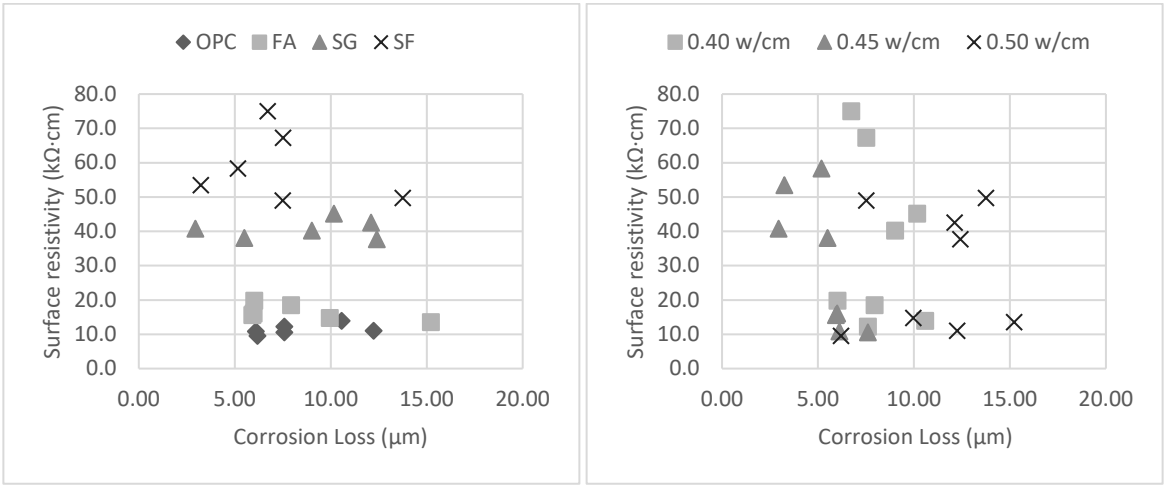

(a) (b)

Figure 49. Graph. Surface resistivity versus corrosion loss: (a) comparison between mixtures of different SCMs and (b) mixtures of varying w/cm ratios.

Here the performance of a concrete mixture in resisting corrosion initiation is of interest as it is believed to correlate well with the electrical resistivity of concrete. As previously discussed, w/cm ratio was the leading parameter improving corrosion resistance with both 0.4 w/cm ratio and 0.45 w/cm ratio presenting lower trends in total corrosion rate and corrosion loss (Figures 48 and 49). There is no clear trend between the performance of these mixtures and their corresponding resistivity value at 56 days of curing. All mixtures containing SCMs exhibited a similar performance, which is also statistically similar to OPC mixtures. In this case, the recommended levels of chloride ion penetrability were not adequate in predicting the mixtures' performance for the macrocell corrosion test.

Based on the results of this experimental program, surface resistivity is not a good indicator for differing durability mechanisms. Although most durability mechanisms derive from or are supported by a form of physical or chemical transport mechanism, electrical resistivity alone does not seem to provide an indication of these phenomena, as it does not correlate with physical transport parameters such as rate of absorption and percent absorption. (Hartell, 2020).

CHAPTER 4: SURFACE RESISTIVITY LABORATORY TRIAL TESTING

Hartell (2020) determined that w/cm ratio and SCM addition are the prevailing parameters affecting the outcome of a resistivity test. Meanwhile, through statistical analysis, aggregate gradation type and air entrainment may not have a significant effect on resistivity with respect to their control for a given w/cm ratio (Hartell, 2020). However, a variance in aggregate minerology may have an altering effect for certain mixtures, demonstrating the sensitivity of the test method to chemical interactions between solid phases and the electrolyte present in the pore structure. The chemical composition of the pore solution (electrolyte) will have a significant impact on the conductivity of the material. This is where resistivity can be corrected by applying a formation factor to unify measurements between mixtures and isolate the influence of the pore structure alone. This relies on the assumptions that the solid medium is nonconductive (does not influence the electron path during the test) and knowledge is accurate of the resistivity of the saturating medium (i.e., resistivity of the pore solution at the time of the test). For concrete material, both assumptions are difficult to interpret and evaluate due to the material's complex physicochemical properties. However, the electrical conductivity of a material is an inherent property and should not change under set test parameters. This is where the test method can be a useful tool as part of a quality control and quality assurance (QC/QA) program.

To evaluate the ability of a DOT to implement resistivity as part of their test program, two studies were conducted. First, an interlaboratory trial was performed to evaluate the consistency in performing the test method between DOT districts. Second, a field trial evaluation of different mixture designs was performed.

INTERLABORATORY TRIAL

A training workshop on surface resistivity testing was held at the IDOT Central Bureau of Materials concrete laboratory. The objective of this workshop was to provide training on the principles of electrical resistivity and operation training using the Proceq resistivity meter. The concrete cylinders used for the training session were cast by IDOT personnel at their facilities (Figures 50 and 51). Three groups of personnel from different IDOT divisions participated by conducting a series of tests on samples.

(a) (b)

Figure 50. Photo. (a) Concrete mixing and (b) sample preparation at IDOT's materials laboratory.

(a) (b)

Figure 51. Photo. (a) Resistivity training and (b) day 1 resistivity testing at the workshop.

Three OPC concrete mixtures of varying water-to-cementitious material ratios (0.4, 0.45, and 0.5) were prepared. Each batch consisted of 15 Ø100 × 200 mm (Ø4 × 8 in.) concrete cylinders. The concrete samples were demolded after 20 hours of curing in their molds. Immediately after demolding the specimens, each group of participants measured, marked, and tested three specimens from each batch, and recorded the data in the provided data entry sheet as the day 1 resistivity results. Afterwards, the samples were transported to their respective districts and immersed in a limewater bath for the rest of the test period. A sample set was also transported to Texas A&M University to be tested. Resistivity measurements were taken on days 7, 14, 28, and 49 from the fabrication date. Note that the day 49 measurement was not taken on the same date across all districts, contributing to the variability in results. Figures 52 to 54 demonstrate the time-resistivity curves for all three mixtures based on the average resistivity value of the three replicates.

On day 1, all district personnel performed the test procedure well and independently. Under the same laboratory conditions and sample temperature, all results are statistically similar for samples X26 and X27. However, District 4 recorded a slightly higher value for X28 that is considered statistically significant. This trend continued throughout the test period. There is no explanation as to why this particular set of samples recorded higher resistivity.

For days 7, 14, and 28, Districts 1 and 3 are consistent with TAMU measurements, while the Central Bureau of Materials lab and District 4 recorded higher values. The temperature of the specimens was taken at the time of the test. Temperatures for District 1 varied between 20.6°C and 23.9°C (69.0°F and 75.0°F), which is considered acceptable. Temperatures for District 3 varied between 20.6°C and 23.9°C (65.0°F and 73.0°F) but were maintained below 21.1°C (70.0°F) for the majority of the test period. This may be a little lower than desired, as surface temperature of concrete can influence the results under standard testing conditions. Temperatures for District 4 varied between (71.0°F and 77.0°F) but were generally maintained near 22.8°C (73.0°F), which is considered optimal. Still, the difference in temperature between District 3 and District 4 labs did not have a significant impact on the outcome of the study. However, these are considered extremes, and ambient lab conditions near 22.8°C (73.0°F) should be encouraged.

Part of the operator comments provided was to adjust to surface wetting and to ensure that the probes were not overly saturated at the beginning of a test. The operators noticed that too much

water on the surface of the concrete cylinder led to variable results. This form of procedural variability could have accounted for the slight differences encountered in the data. This can be adjusted with continued practice and familiarity of the method.

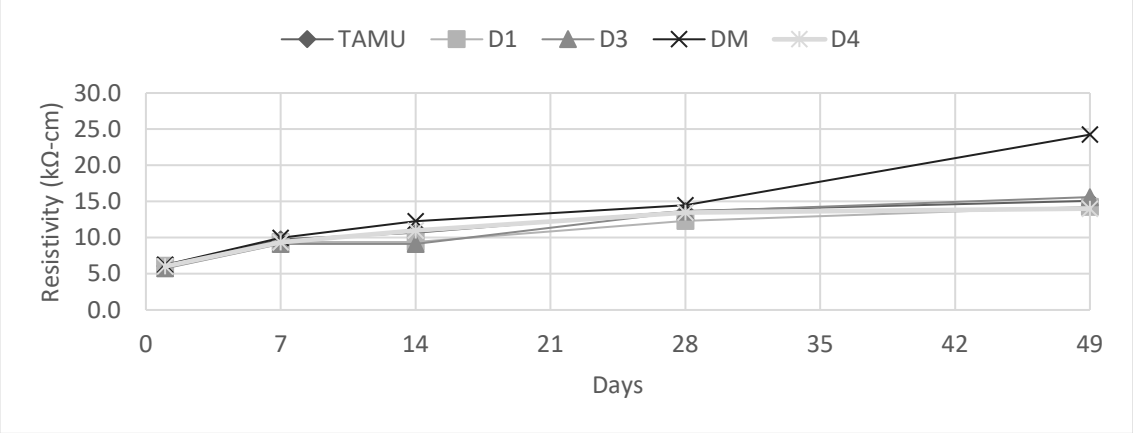

Figure 52. Graph. District results for resistivity over time for mixture design X26: OPC, 0.5 w/cm ratio.

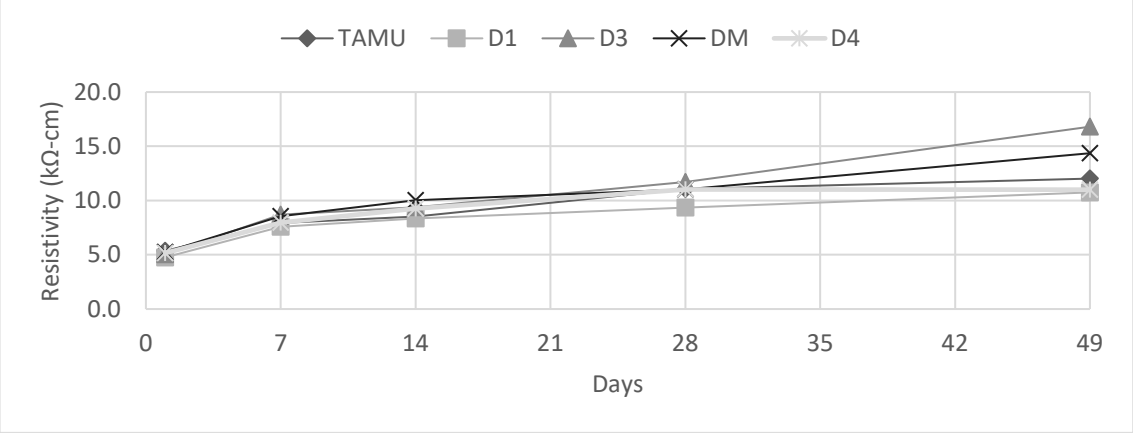

Figure 53. Graph. District results for resistivity over time for mixture design X27: OPC, 0.45 w/cm ratio.

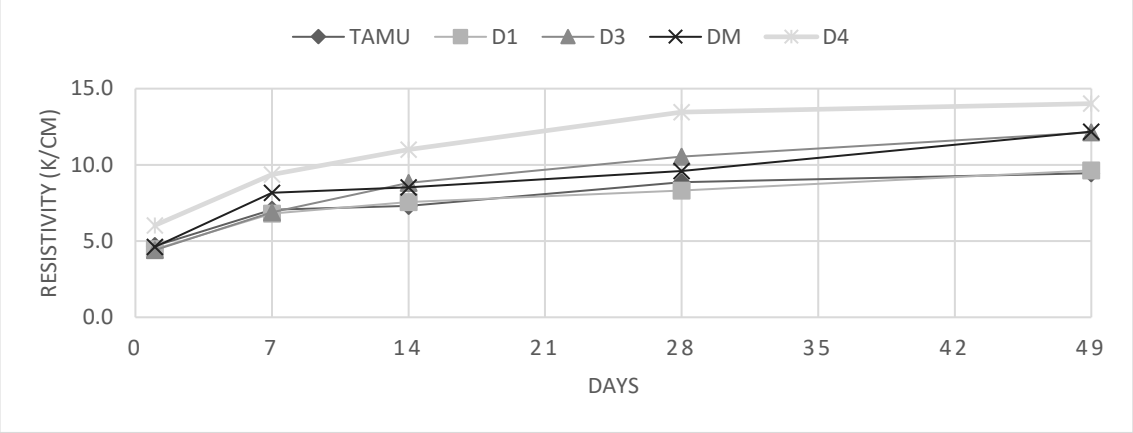

Figure 54. Graph. District results for resistivity over time for mixture design X28: OPC, 0.40 w/cm ratio.

INDEPENDENT LABORATORY RESISTIVITY DATA

For this project, an independent laboratory provided a series of mixture designs typically used for pavement construction. The concrete mixtures are fabricated with blends of Class C fly ash and slag cement as well as various aggregate blends providing an optimized gradation for pavement construction. Resistivity testing was performed on days 28, 56, and 91 to determine the resistance to chloride ion penetrability (CIP) in accordance with AASHTO T 358. At 28 days, all mixtures achieved a moderate to low classification of penetrability potential. However, only after 91 days of curing did all mixtures achieve a low classification level, which is the desired classification. As previously discussed, the early age rate in resistivity gain provides additional insight on a mixture's potential to achieve a higher classification level at a later age. Although this information is not provided, the 28 to 91 day trend exhibited in Figure 55 provides an indication that the mixtures of various SCM blends behaved in a similar manner. Mixture design information is provided in Appendix B along with the results of the electrical resistivity investigation for the 45 concrete designs. This section presents a select data set for the purpose of discussion.

The gain in resistivity over time for a standard concrete mixture is influenced by the type and content of cementitious and pozzolanic materials. As such, the data set provided was divided into four categories: 0% FA–35% SG, 10% FA–25% SG, 15% FA–20% SG, and 27% FA–12% SG. One mixture containing a 35% slag cement replacement and four ternary mixtures of varying fly ash and slag cement contents.

As demonstrated in Figure 55, the four mixture categories present varying rates in resistivity gain. The greatest rate in resistivity gain is for the 27% FA–12% SG mixture, which may be attributed to the total SCM replacement of 39% versus 35% for the other three mixtures. The aggregate source and paste content may also influence this behavior. Therefore, the data set was subsequently divided into mixtures of similar characteristics to compare their resistivity behaviors.

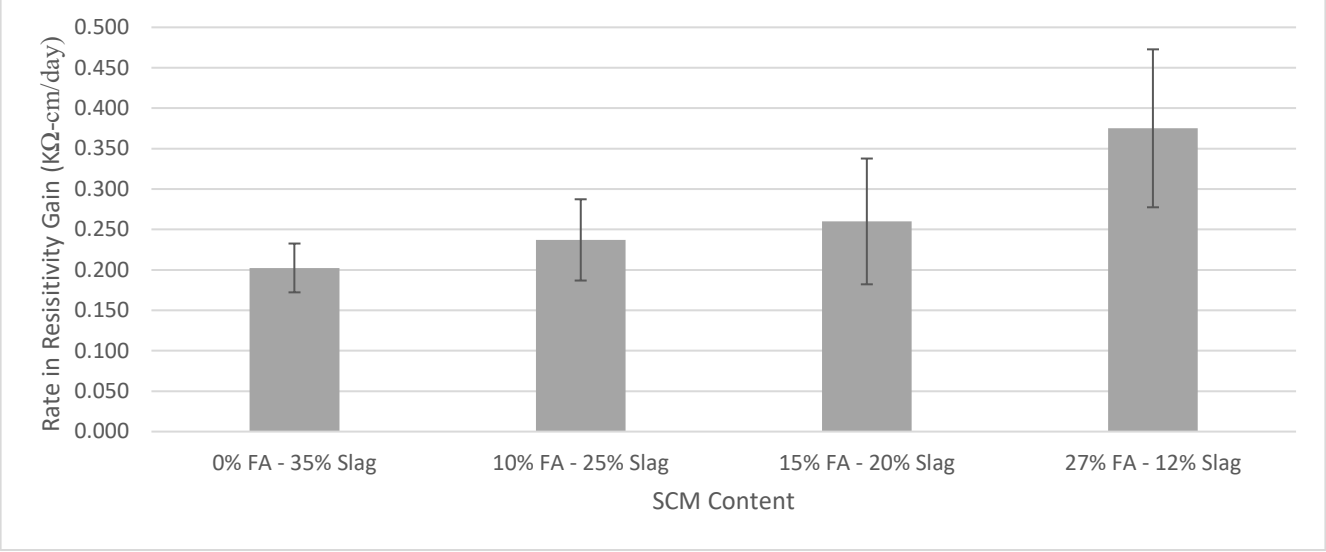

Figure 55. Graph. 28 to 91 day rate in surface resistivity gain for mixtures of varying % SCM content.

Concrete Mixtures with 27% Fly Ash and 12% Slag Cement

Starting with the 27% FA–12% SG blend presented in Table 5, Figure 56 demonstrates that the resistivity values are distinct. However, the gain in resistivity over time follows a similar trend. In fact, the mixture designs demonstrate a high potential for resistivity gain over time, making these mixtures of very low conductivity.

To further differentiate the mixtures, aggregate properties were compared. Mixtures 10 and 11, 8 and 9, and 14 and 15 were found to have similarities. Figure 57 compares the individual set of results. For all three pairs, the average resistivity values are considered statistically similar based on the assumption of a maximal 6.8% coefficient of variation.

Table 5. Mixture Design Information for Mixtures Containing 27% Fly Ash and 12% Slag Cement

	Resistivity (kΩ-cm)			Resistivity Rate Gain	SCM		Materials (lb)					
Mix ID	Day 28	Day 56	Day 91	Days 28 to 91	FA (%)	SLAG (%)	Total CM	CA1	CA2	FA	Air	w/c
10	20.9	26.8	34.7	0.399	27	12	565	1340	500	1345	6.5	0.393
11	26.4	34.7	45.3	0.417	27	12	565	1340	500	1345	6.5	0.393
08	17.8	31.1	42.6	0.582	27	12	565	1385	458	1345	6.5	0.393
09	15.5	27.9	41.5	0.627	27	12	565	1385	458	1345	6.5	0.393
12	28.0	–	78.9	0.645	27	12	565	1392	445	1350	6.5	0.393
13	19.8	34.5	–	–	27	12	565	1392	448	1350	6.5	0.393
14	26.9	45.0	57.5	0.531	27	12	565	1733	135	1335	6.5	0.393
15	23.6	38.9	51.4	0.540	27	12	565	1733	135	1335	6.5	0.393

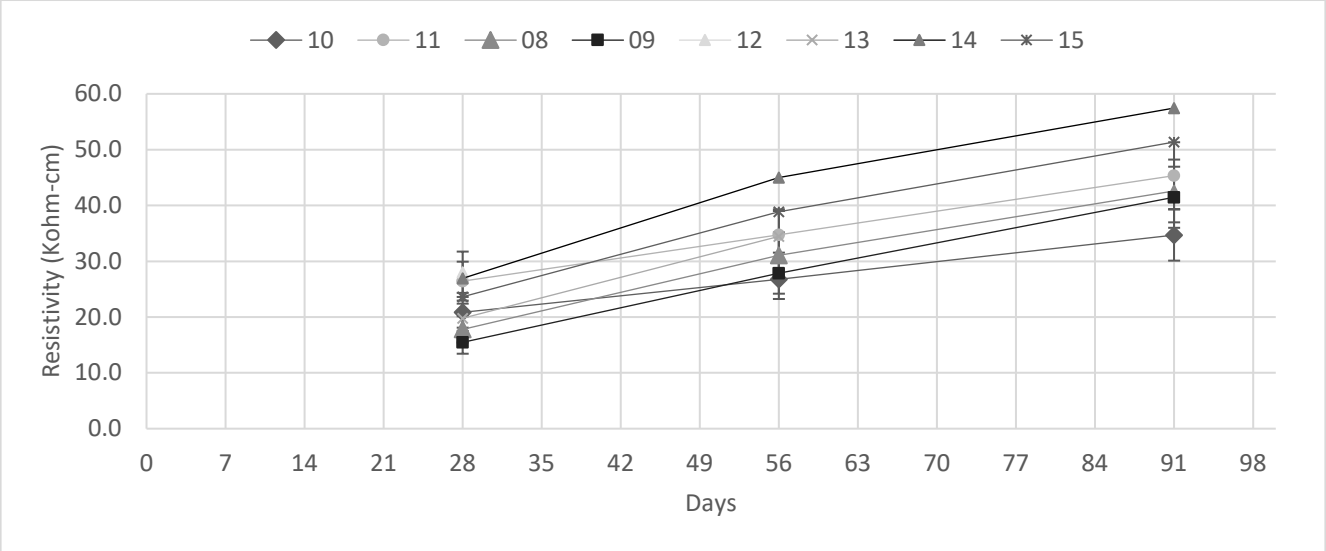

Figure 56. Graph. Gain in surface resistivity over time for mixtures containing 27% FA and 12% slag.

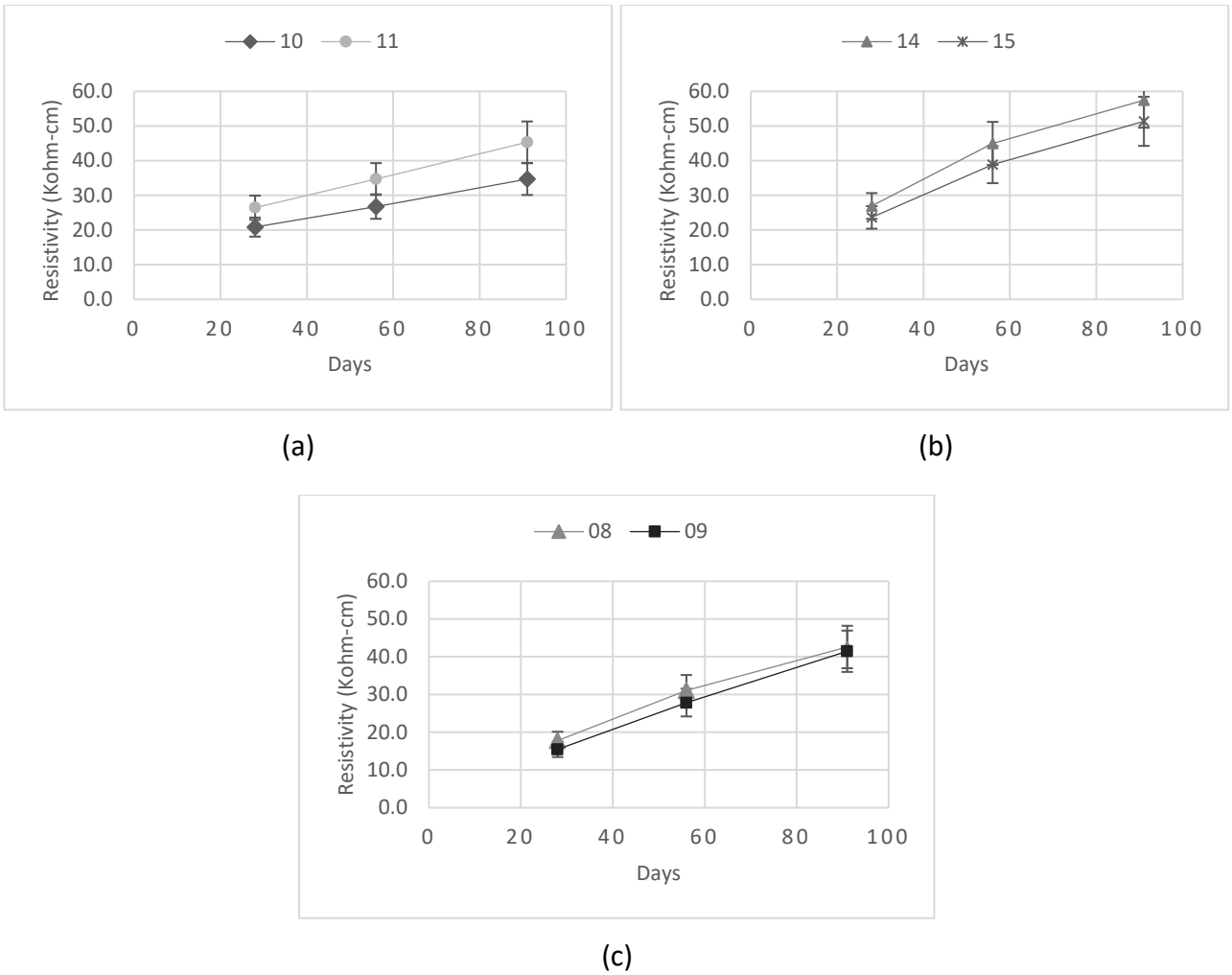

Figure 57. Graph. Gain in surface resistivity over time for mixtures containing 27% FA and 12% slag; comparison for three different aggregate blends.

Concrete Mixtures with 15% Fly Ash and 20% Slag Cement

The results for mixtures containing 15% fly ash and 20% slag cement are presented in Table 6. The resistivity behaviors are presented in Figure 58. The gain in resistivity over time slightly varies for the 15 mixtures, making them statistically distinct. Looking at commonalities in other mix design parameters, the mixtures of similar designs present statistically similar values, as seen in Figure 59.

Table 6. Mixture Design Information for Mixtures Containing 15% Fly Ash and 20% Slag Cement

	Resistivity (kΩ-cm)			Resistivity Rate Gain	SCM		Materials					
Mix ID	Day 28	Day 56	Day 91	Days 28 to 91	FA (%)	SLAG (%)	Total CM	CA1	CA2	FA	Air	w/c
39	15.5	24.1	25.3	0.048	15	20	605	1366	514	1141	6.5	0.421
07	15.1	21.9	28.3	0.226	16	20	580	1667	250	1213	6.0	0.391
36	14.4	21.0	26.6	0.212	15	20	605	1606	243	1184	6.0	0.420
35	14.9	20.8	27.6	0.244	14	21	575	1420	390	1270	6.5	0.420
38	13.7	17.7	24.6	0.281	14	21	575	1430	390	1280	6.5	0.420
46	15.6	25.6	35.1	0.269	15	20	495	1459	420	1327	6.0	0.455
45	15.7	26.4	38.0	0.306	15	21	535	1420	429	1308	6.0	0.430
42	16.0	26.6	42.1	0.369	15	20	605	1764	182	1085	6.0	0.421
24	19.0	27.1	31.6	0.144	15	21	535	1911	–	1251	6.5	0.402
37	17.8	26.1	31.8	0.180	14	21	575	1400	400	1265	6.5	0.420
25	20.7	29.3	38.5	0.239	16	21	580	1630	264	1160	6.5	0.407
31	17.8	28.1	34.3	0.181	14	21	605	1399	376	1235	6.5	0.420
06	16.0	22.5	34.9	0.353	16	20	580	1667	250	1213	6.0	0.390
43	17.9	25.0	33.5	0.254	15	20	605	1606	243	1184	6.0	0.421
41	17.8	30.0	41.6	0.277	16	20	580	1733	216	1133	6.0	0.421

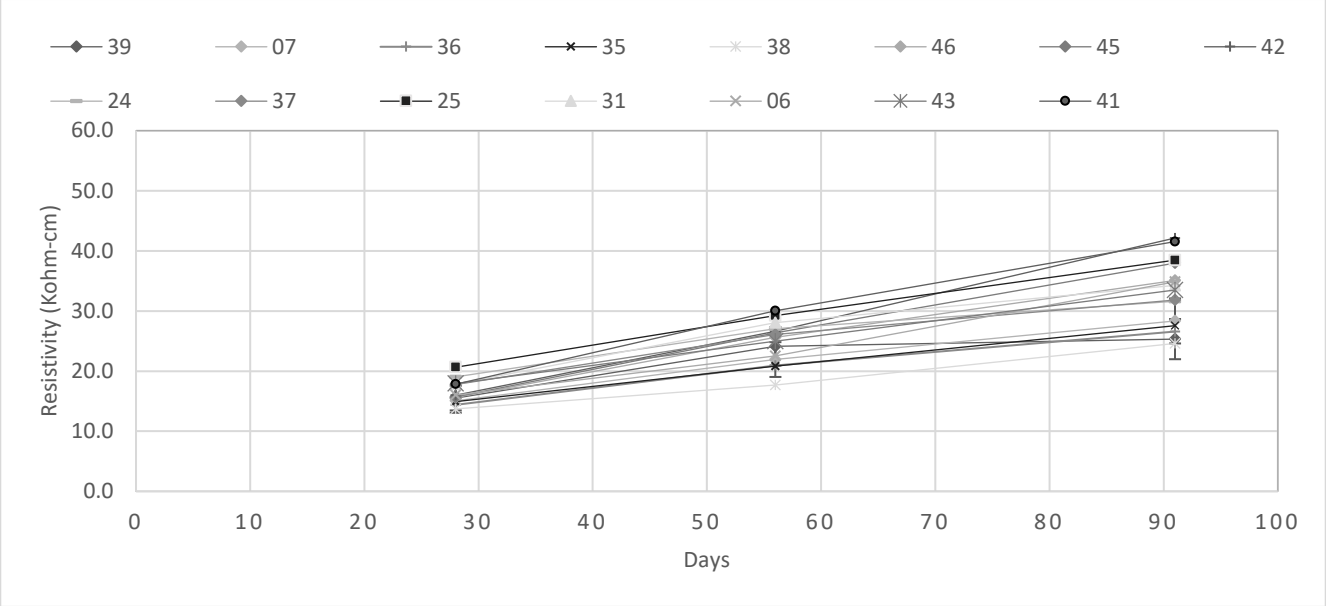

Figure 58. Graph. Gain in surface resistivity over time for mixtures containing 15% FA and 20% slag.

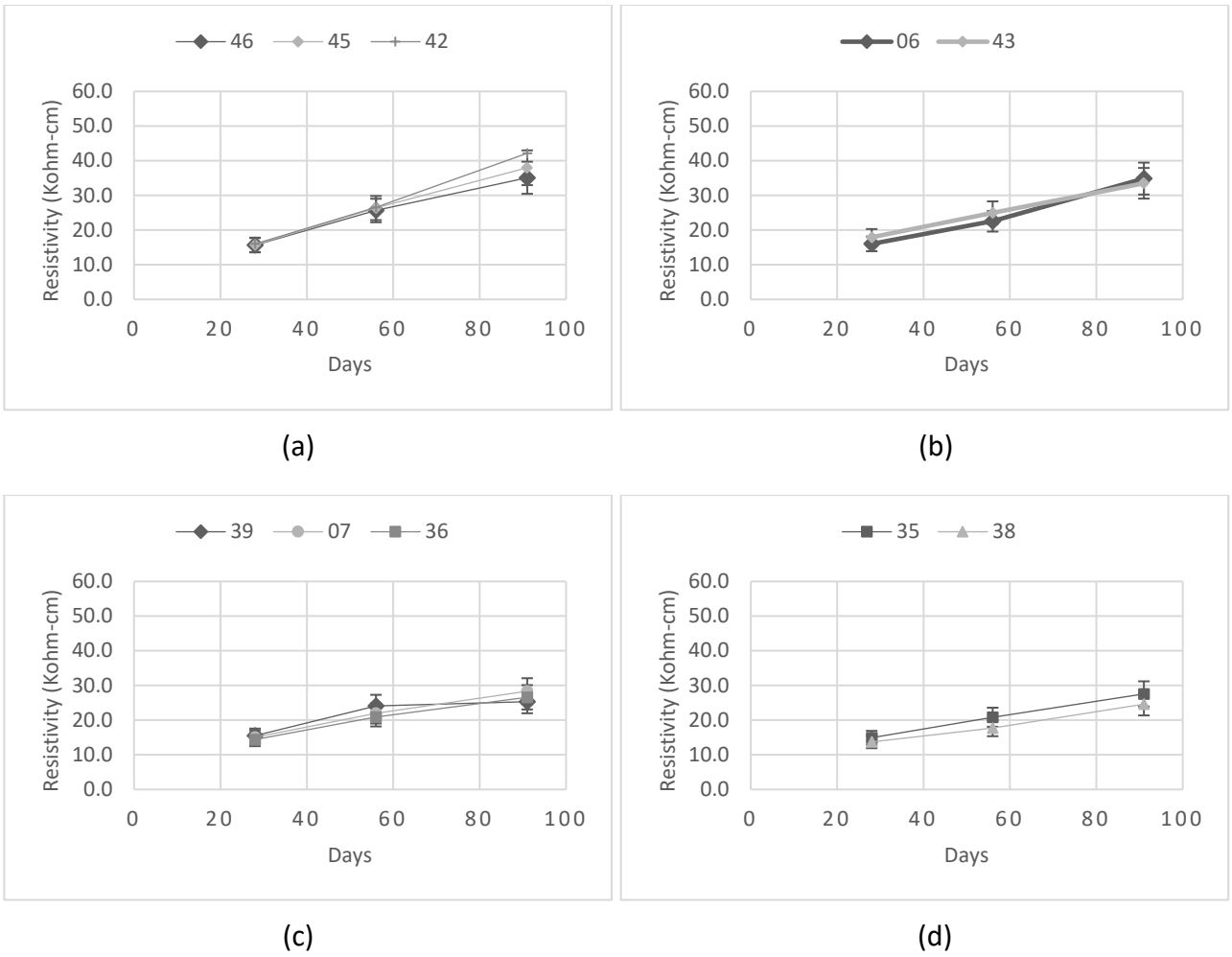

Figure 59. Graph. Gain in surface resistivity over time for mixtures containing 15% FA and 20% slag; comparison for four different aggregate blends.

Concrete Mixtures with 10% Fly Ash and 25% Slag Cement

The results for the mixtures containing 10% fly ash and 25% slag are reported in Table 7. Similar to the previous mixture designs, the eight 10% FA–25% SG mixtures slightly vary in resistivity behavior over time (Figure 60). In fact, the results between the 15% FA–20% SG and 10% FA–25% SG are comparable. This agrees with findings previously reported by Hartell (2020), where a 5% to 10% change in SCM content may not be statistically discernable but an increase in total SCM content will present a higher resistivity gain. For this set, three mixture pairs were found to have similar characteristics and their comparison is presented in Figure 61. The pairs are statistically similar.

Table 7. Mixture Design Information for Mixtures Containing 10% Fly Ash and 25% Slag Cement

	Resistivity (kΩ-cm)			Resistivity Rate Gain	SCM		Materials					
Mix ID	Day 28	Day 56	Day 91	Days 28 to 91	FA (%)	SLAG (%)	Total CM	CA1	CA2	FA	Air	w/c
27	20.3	29.4	34.3	0.409	12	23	520	1500	450	1300	6.5	0.417
30	17.6	24.5	30.9	0.432	12	23	535	1500	450	1280	6.5	0.420
28F	17.5	25.7	33.9	0.483	10	25	670	1460	320	1130	6.5	0.419
26F	17.6	28.2	36.3	0.515	10	25	625	1490	350	1179	6.5	0.409
29F	18.2	26.6	36.2	0.498	10	25	535	1408	414	1320	6.5	0.420
40	16.1	21.3	25.5	0.367	10	25	580	1386	522	1157	6.5	0.421
44	15.9	22.4	–	–	10	25	580	1386	522	1165	6.5	0.421
18	16.7	28.0	31.4	0.469	10	25	580	1478	465	1154	6.5	0.400

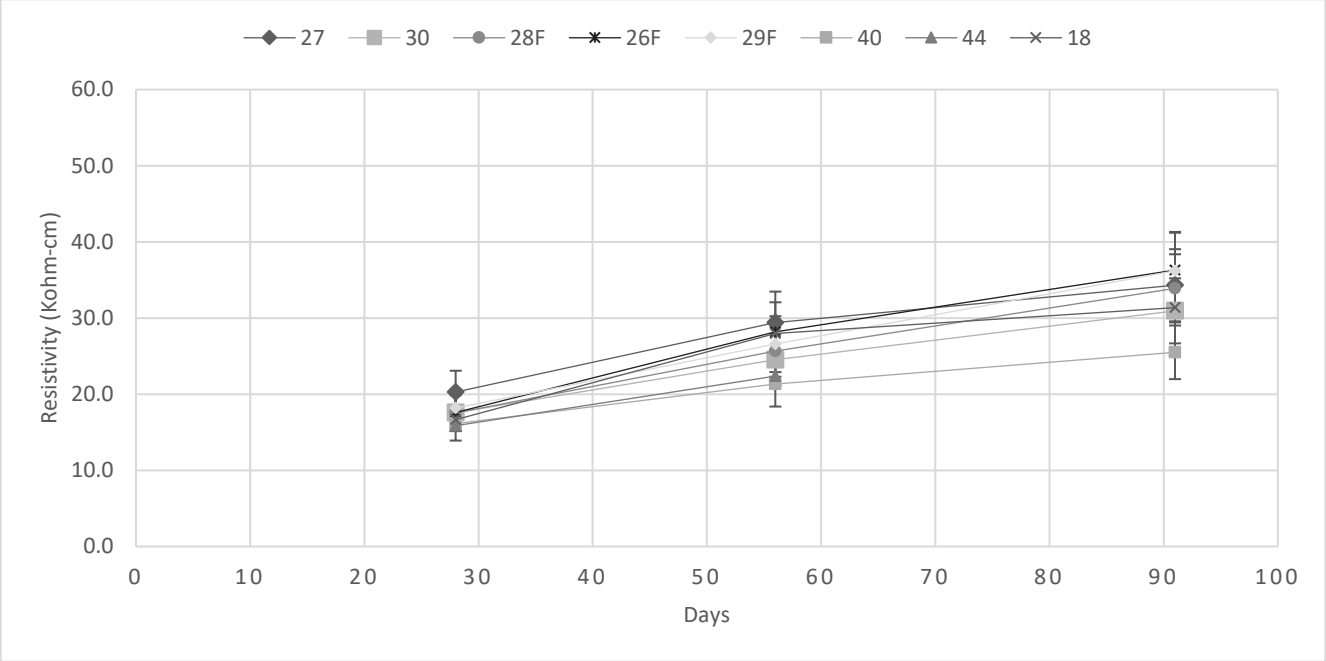

Figure 60. Graph. Gain in surface resistivity over time for mixtures containing 10% FA and 25% slag.

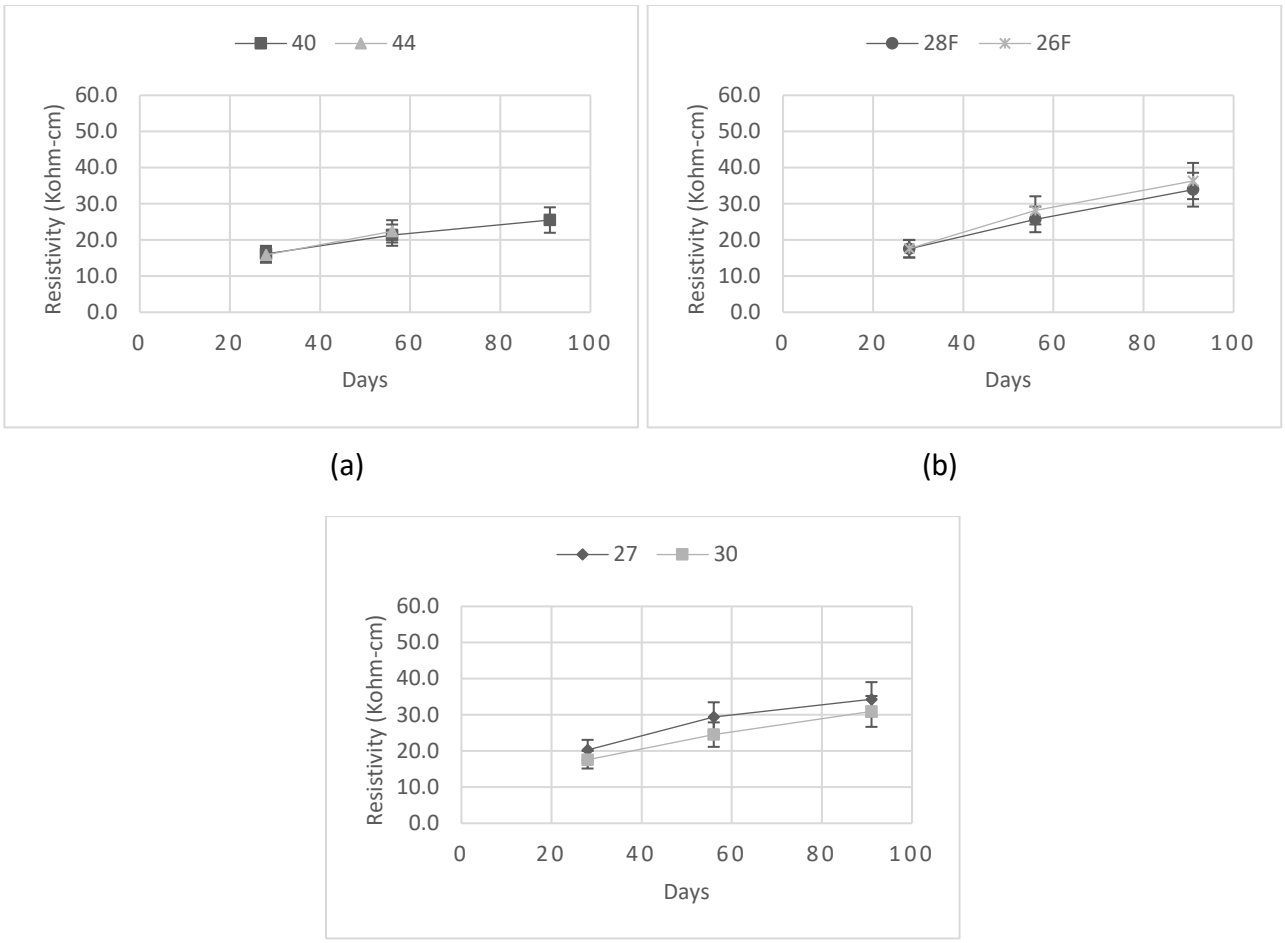

Figure 61. Graph. Gain in surface resistivity over time for mixtures containing 10% FA and 25% slag; comparison for three different aggregate blends.

Concrete Mixtures with 0% Fly Ash and 35% Slag Cement

Six mixtures containing slag cement replacement only were part of this study. Table 8 and Figure 62 present the resistivity results. The results for the majority of the mixtures are statistically similar, and they are comparable in behavior to that obtained for the 40% slag mixtures previously reported. Figure 63-A demonstrates that mixtures 17, 19, and 22 obtained the same results for the test period; however, the difference between mixtures 20 and 21 is considered statistically different (Figure 63-B). Although the aggregate properties for the latter mixtures appear to be similar, further information would be required to provide a sound justification for the differences.

Table 8. Mixture Design Information for Mixtures Containing 0% Fly Ash and 35% Slag Cement

	Resistivity (kΩ-cm)			Resistivity Rate Gain	SCM		Materials					
Mix ID	Day 28	Day 56	Day 91	Days 28 to 91	FA (%)	SLAG (%)	Total CM	CA1	CA2	FA	Air	w/c
20	20.2	30.1	35.7	0.434	0	35	535	1475	442	1268	6.5	0.400
21	17.0	23.5	27.7	0.387	0	35	535	1475	442	1268	6.5	0.400
22	19.6	25.9	31.5	0.378	0	35	535	1390	547	1260	6.5	0.400
19	19.7	25.6	31.5	0.373	0	35	535	1368	547	1251	6.5	0.400
17	19.8	26.0	–	–	0	35	535	1368	547	1260	6.5	0.400
23	22.9	30.0	36.8	0.377	0	36	535	1411	500	1275	6.5	0.402

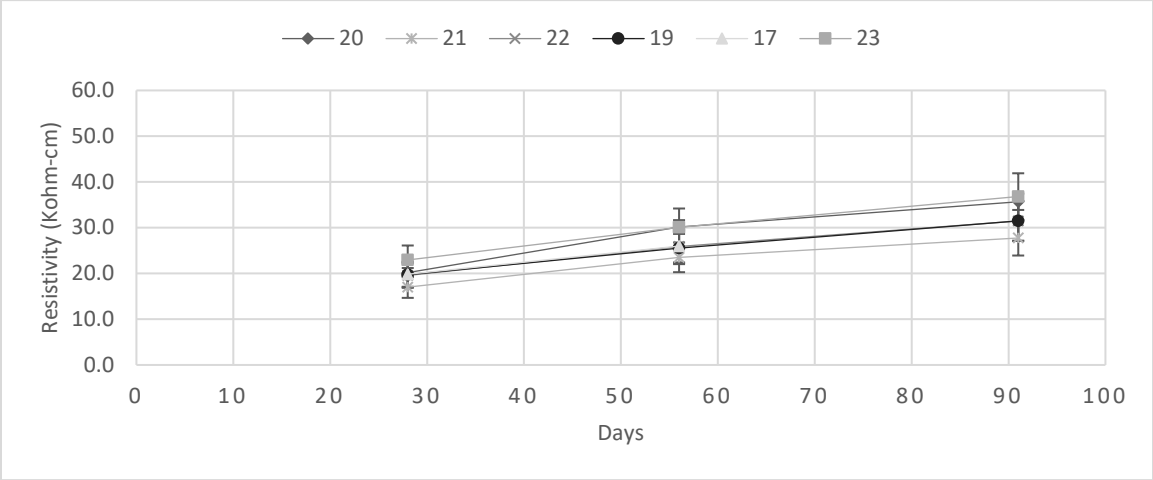

Figure 62. Graph. Gain in surface resistivity over time for mixtures containing 0% FA and 35% slag.

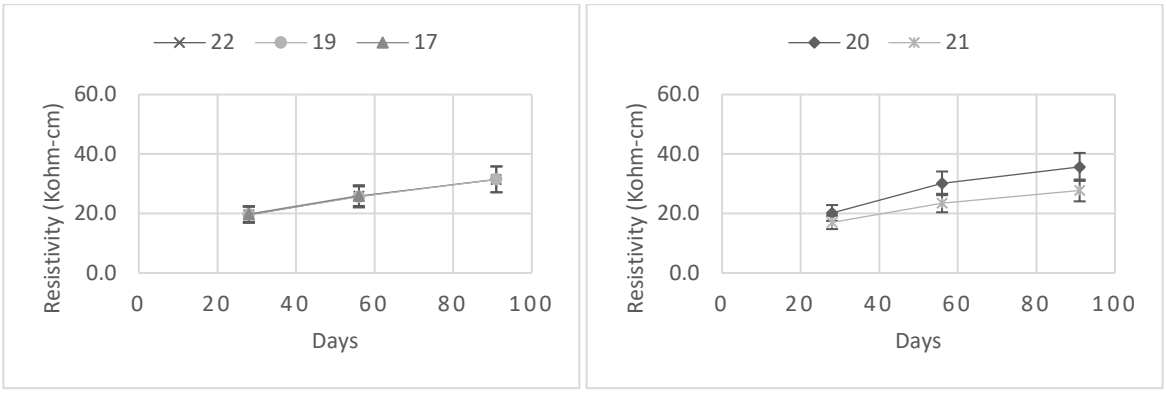

(a) (b)

Figure 63. Graph. Gain in surface resistivity over time for mixtures containing 0% FA and 35% slag; comparison for three different aggregate blends.

CHAPTER 5: CONCLUSIONS

Although classification tables based on susceptibility to chloride ion permeability are recommended in AASHTO T 358, the classification levels with respect to durability parameters may or may not be adequate. The application of correction factors such as the formation factor is recommended to provide a better assessment of concrete's porosity characteristics (i.e., physical transport properties). Determining pore solution chemistry is a cumbersome procedure, however, that may be difficult to implement as part of a routine QC/QA program. Still, the results may not be meaningful when comparing with actual durability test results. This fact poses a problem when designing a concrete pavement mixture based on performance measures. Optimization in SCM replacements and admixture additions may not be reflected through resistivity testing. Implementation of AASHTO TT 84 must be evaluated carefully when it comes to resistivity testing to determine the performance of a mixture.

Of interest for concrete pavement performance, this study verifies the method against actual durability testing such as corrosion, salt scaling, and freeze-thaw. These durability tests were conducted in parallel with electrical surface resistivity testing to compare performance classifications for each method. Resistivity did not correlate with any of the durability tests performed. In some cases, it was counterintuitive where mixtures of low resistivity performed better than mixtures of high resistivity.

Such is the case for salt-scaling performance of concrete mixtures containing SCMs. Although the mixtures recorded high resistivity values, which is an indication of improved resistance to chloride diffusion transport properties, concrete samples containing SCMs demonstrated an increased level of surface damage compared to OPC samples. The OPC sample with a 0.5 w/cm ratio behaved better than the samples containing SCMs with a 0.4 w/cm ratio. Fly ash was the most detrimental to scaling performance. Still, a low w/cm ratio combined with air entrainment produced an acceptable performance.

For freeze-thaw testing, mixtures of very low to moderate CIP classification passed the performance parameters for freeze-thaw durability. There is no correlation between the obtained durability factor and the 56-day resistivity. Adequate air entrainment was the dominating parameter followed by SCM addition and low w/cm ratio.

The results of the macrocell corrosion test also demonstrated adequate performance at the end of the 15-week test period. The dominating factor improving the performance was w/cm ratio followed by the addition of SCMs; however, there is not a clear distinction on performance for this rapid method of testing. The CIP classification did not provide an indication of mixture performance to corrosion, as the results did not yield an obvious correlation.

The use of resistivity testing can still be a good tool as part of a QC/QA program, if performed correctly and with an understanding of its capabilities. They take only a few seconds to run and can be performed on existing cylinders meant for standard compression testing. The simplicity of the test method ensured reproducible results between four district laboratories conducting the AASHTO T

358 test method on samples fabricated from the same concrete batches. Small procedural errors may have been attributed to surface wetting and specimen temperature inconsistencies. Both parameters can easily be corrected with operator experience and careful maintenance of ambient laboratory conditions and curing temperatures.

The comparative assessment of resistivity results for 45 concrete mixtures produced by an independent laboratory provided insight on the potential implementation of the resistivity method suggested by Hartell (2020). It was found that mixtures of similar composition and mixture design can yield the same results. This fact can be helpful, as resistivity behavior over time should be the same under the same condition for a given concrete mixture. If the starting chemistry and hydration development is the same over time, a test method sensitive to physico-chemical properties of a material should be adequate. Therefore, it is recommended that a resistivity-time curve be provided during mixture design acceptance. This curve can be used as part of the QC/QA process during construction as a comparative assessment tool. Substantial deviations from the approved design could be an indication of a change in mixture parameters for the concrete delivered on-site. A negative impact such as increased water content or improper SCM quantities could result in decreased performance of the constructed pavement.

REFERENCES

AASHTO TP 95. (2014). *Standard test method for surface resistivity of concrete's ability to resist chloride ion penetration*. American Association of State Highway and Transportation Officials.

AASHTO TP 119 (2017). *Standard test method for electrical resistivity of concrete cylinder tested in a uniaxial resistance test*. American Association of State Highway and Transportation Officials.

AASHTO T 358. (2015). *Standard test method for surface resistivity of concrete's ability to resist chloride ion penetration*. American Association of State Highway and Transportation Officials.

Álava, H. E, De Belie, N., & De Schutter, G. (2016). Proposed mechanism for the formation of oxychloride crystals during sodium chloride application as a deicer salt in carbonated concrete. *Construction and Building Materials*, *109*, 188–197.

ASTM Standard C192-16a (2016). *Standard practice for making and curing concrete test specimens in the laboratory*. ASTM International.

ASTM Standard C127-15 (2015). *Standard test method for relative density (specific gravity) and absorption of coarse aggregate*. ASTM International.

ASTM Standard C128-15 (2015). *Standard test method for relative density (specific gravity) and absorption of fine aggregate*. ASTM International.

ASTM Standard C138-17a (2017). *Standard test method for density (unit weight), yield, and air content (gravimetric) of concrete*. ASTM International.

ASTM Standard C143-20 (2020). *Standard test method for slump of hydraulic-cement concrete*. ASTM International.

ASTM Standard C150-21 (2021) *Standard specification for Portland cement*. ASTM International.

ASTM Standard C192-19 (2019). *Standard practice for making and curing concrete test specimens in the laboratory*. ASTM International.

ASTM Standard C215-19 (2019) *Standard test method for fundamental transverse, longitudinal, and torsional resonant frequencies of concrete specimens*. ASTM International.

ASTM Standard C231-17a (2017) *Standard test method for air content of freshly mixed concrete by the pressure method*. ASTM International.

ASTM Standard C511-21 (2021). *Standard specification for mixing rooms, moist cabinets, moist rooms, and water storage tanks used in the testing of hydraulic cements and concretes*. ASTM International.

ASTM Standard C666-15 (2015). *Standard test method for resistance of concrete to rapid freezing and thawing*. ASTM International.

ASTM Standard C1202-19 (2019). *Standard test method for electrical indication of concrete's ability to resist chloride ion penetration*. ASTM International.

ASTM Standard C1760-12 (2012). *Standard test method for bulk electrical conductivity of hardened concrete*. ASTM International.

BNQ NQ 2621-900 (2002). *Determination of the scaling resistance of concrete surfaces exposed to freezing-and-thawing cycles in the presence of de-icing chemicals*. Bureau de Normalisation du Québec, Annexe A, 19-22.

FM 5-578 (2004). *Florida method of test for concrete resistivity as an electrical indicator of its permeability*. Florida Department of Transportation.

Coussy, O., & Monteiro, P. J. M. (2008). Poroelastic model for concrete exposed to freezing temperatures. *Cement and Concrete Research*, *38*(1), 40–48.

Gulrez, W., & Hartell, J. (2017). Effect of curing condition and temperature on surface resistivity measurements. *Proc., 26th ASNT Research Symposium*, 99–107.

Gulrez, W., & Hartell, J. (2018). New method for quality control and compliance of concrete mixture design using surface resistivity testing. *2018 Transportation Research Board Annual Meeting*.

Gulrez, W., & Hartell, J. (2019). Effect of aggregate type and size on surface resistivity testing. *Journal of Materials in Civil Engineering*, *31*(6), 1–13.

Hartell, J., & Shults, C. (2018). *Surface resistivity testing for quality control of concrete mixtures* (Report No. SPTC 17.1-07). Southern Plains Transportation Center.

Hartell, J. (2020). *The use of surface resistivity testing for quality control of concrete mixtures* (Report No. FHWA-OK-20-03). Oklahoma State University, Oklahoma Department of Transportation.

Hooton, D., & Vassilev, D. (2012). *Deicer scaling resistance of concrete mixtures containing slag cement; Phase 2: Evaluation of different laboratory scaling test methods* (Report No. DTFH61-06-H-00011 Work Plan 24). Iowa State University, Institute for Transportation.

Jones, C., Ramanathan, S., Suraneni, P., & Hale, W. M. (2020). Calcium oxychloride: A critical review of the literature surrounding the formation, deterioration, testing procedures, and recommended mitigation techniques. *Cement and Concrete Composites*, *113*, 103663.

Kessler, R. J., Powers, R. G., & Mario Paredes, M. P. (2005). Resistivity measurements of water saturated concrete as an indicator of permeability. Paper presented at CORROSION 2005, Houston, Texas, April 3–7.

Kessler, R. J., Powers, R. G., Vivas, E., Paredes, M. A., & Virmani, Y. P. (2008). Surface Resistivity as an Indicator of Concrete Chloride Penetration Resistance. *Proc., Concrete Bridge Conference*, St. Louis, Missouri 20.

Khan, M. U., Ahmad, S., & Al-Gahtani, H. J. (2017). Chloride-induced corrosion of steel in concrete: An overview on chloride diffusion and prediction of corrosion initiation time. *International Journal of Corrosion*, 1–9.

Li, W., Pour-Ghaz, M., Castro, J., & Weiss, J. (2012). Water absorption and critical degree of saturation relating to freeze-thaw damage in concrete pavement joints. *Journal of Materials in Civil Engineering*, *24*(3), 299–307.

Montemor, M. F., Simões, A. M. P., & Ferreira, M. G. S. (2003). Chloride-induced corrosion on reinforcing steel: From the fundamentals to the monitoring techniques. *Cement and Concrete Composites*, *25*(4-5), 491–502.

Morris, W., Moreno, E., & Sagüés, A. (1996). Practical evaluation of resistivity of concrete in test cylinders using a Wenner array probe. *Cement and Concrete Research*, *26*(12), 1779–1787.

Nadelman, E. I., & Kurtis, K. E. (2014). A resistivity-based approach to optimizing concrete performance. *Concrete International*, *36*(5), 50–54.

Neithalath, N., & Jain, J. (2010). Relating rapid chloride transport parameters of concretes to microstructural features extracted from electrical impedance. *Cement and Concrete Research*, *40*(7), 1041–1051.

Peterson, K., Julio-Betancourt, G., Sutter, S., Hooton, R. D., & Johnston, D. (2013). Observations of chloride ingress and calcium oxychloride formation in laboratory concrete and mortar at 5°C. *Cement and Concrete Research*, *45*, 79–90.

Polder, R., Andrade, C., Elsener, B., Vennesland, Ø., Gulikers, J., Weidert R., & Raupach, M. (2000). Test methods for on-site measurement of resistivity of concrete. *Materials and Structures*, *33*, 603–611.

Power, T. C. (1945). A working hypothesis for further studies of frost resistance of concrete. *Journal of American Concrete Institute*, *41*(1), 245–272.

Rupnow, T., & Icenogle, P. (2012). Surface resistivity measurements evaluated as alternative to rapid chloride permeability test for quality assurance and acceptance. *Transportation Research Record: Journal of the Transportation Research Board*, 2290, 30–37.

Song, H.-W., Lee, C-H., & Ann, K. Y. (2008). Factors influencing chloride transport in concrete structures exposed to marine environments. *Cement and Concrete Composites*, *30*(2), 113–121.

Spragg, R., Bu, Y., Snyder, K., Bentz, D., & Weiss, J. (2013). *Electrical testing of cement-based materials: Role of testing techniques, sample conditioning, and accelerated curing* (Report No. FHWA/IN/JTRP-2013/28). Joint Transportation Research Program, Indiana Department of Transportation.

Stanish, K. D., Hooton, R. D., & Thomas, M. D. A. (2001). Testing the chloride penetration resistance of concrete: A literature review. Department of Civil Engineering, University of Toronto.

Valenza, J. J., & Scherer, G. W. (2006). Mechanism for salt scaling. *Journal of the American Ceramic Society*, *89*(4), 1161–1179.

Valenza, J. J., & Scherer, G. W. (2007). A review of salt scaling: II. Mechanisms. *Cement and Concrete Research*, *37*(7), 1022–1034.

Vollpracht, A., Lothenbach, B., Snellings. R., & Haufe, J. (2016). The pore solution of blended cements: A review. *Materials and Structures*, *49*(8), 3341–3367.

Wang, Y., Liu, Z., Fu, K., Li, Q., & Wang, Y. (2020). Experimental studies on the chloride ion permeability of concrete considering the effect of freeze–thaw damage. *Construction and Building Materials*, 236.

APPENDIX A: RESULTS RESISTIVITY TESTING—ALL MIXTURES

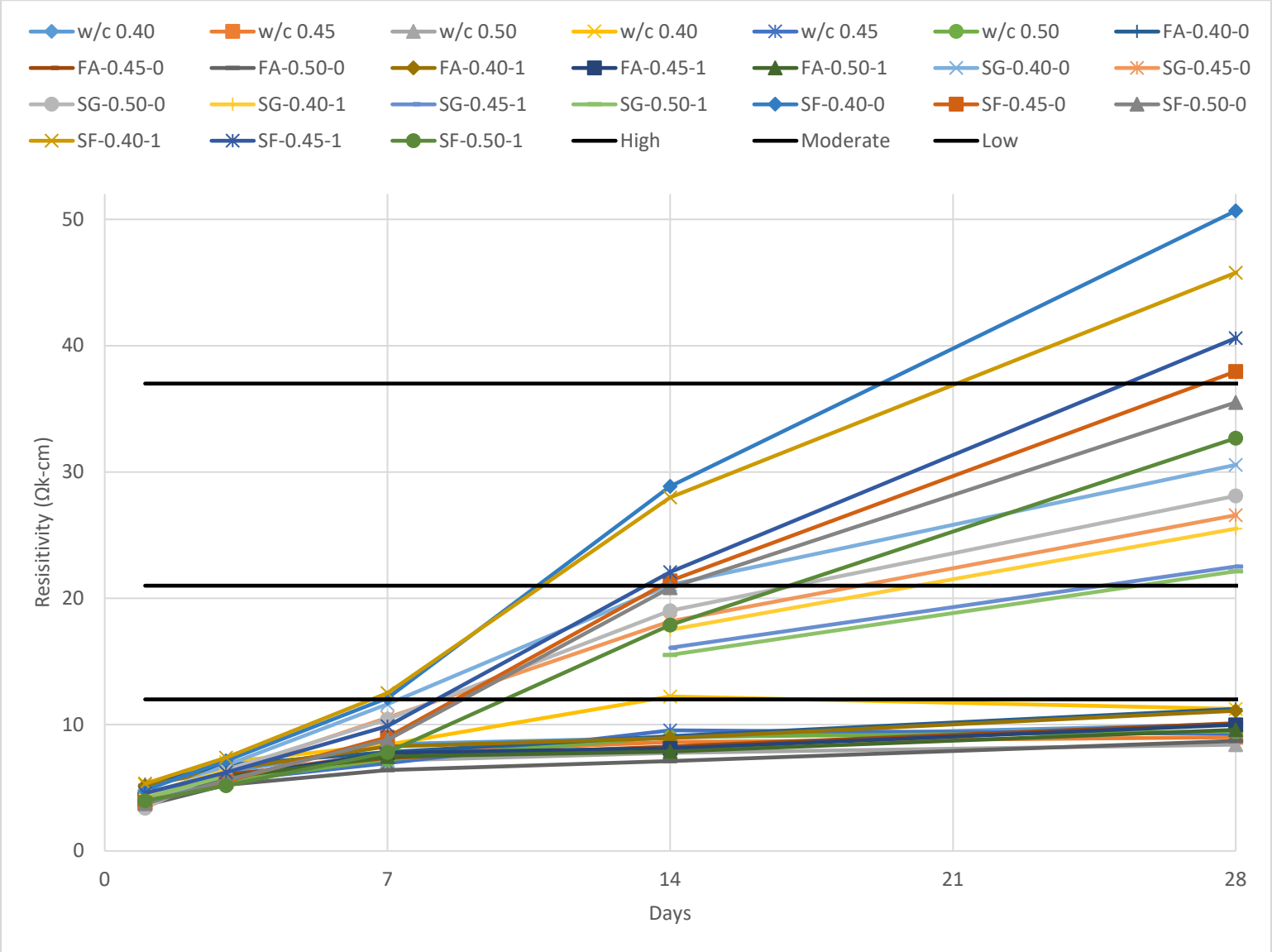

Figure 64. Graph. Gain in surface resistivity up to 28 days for all mixtures designs.

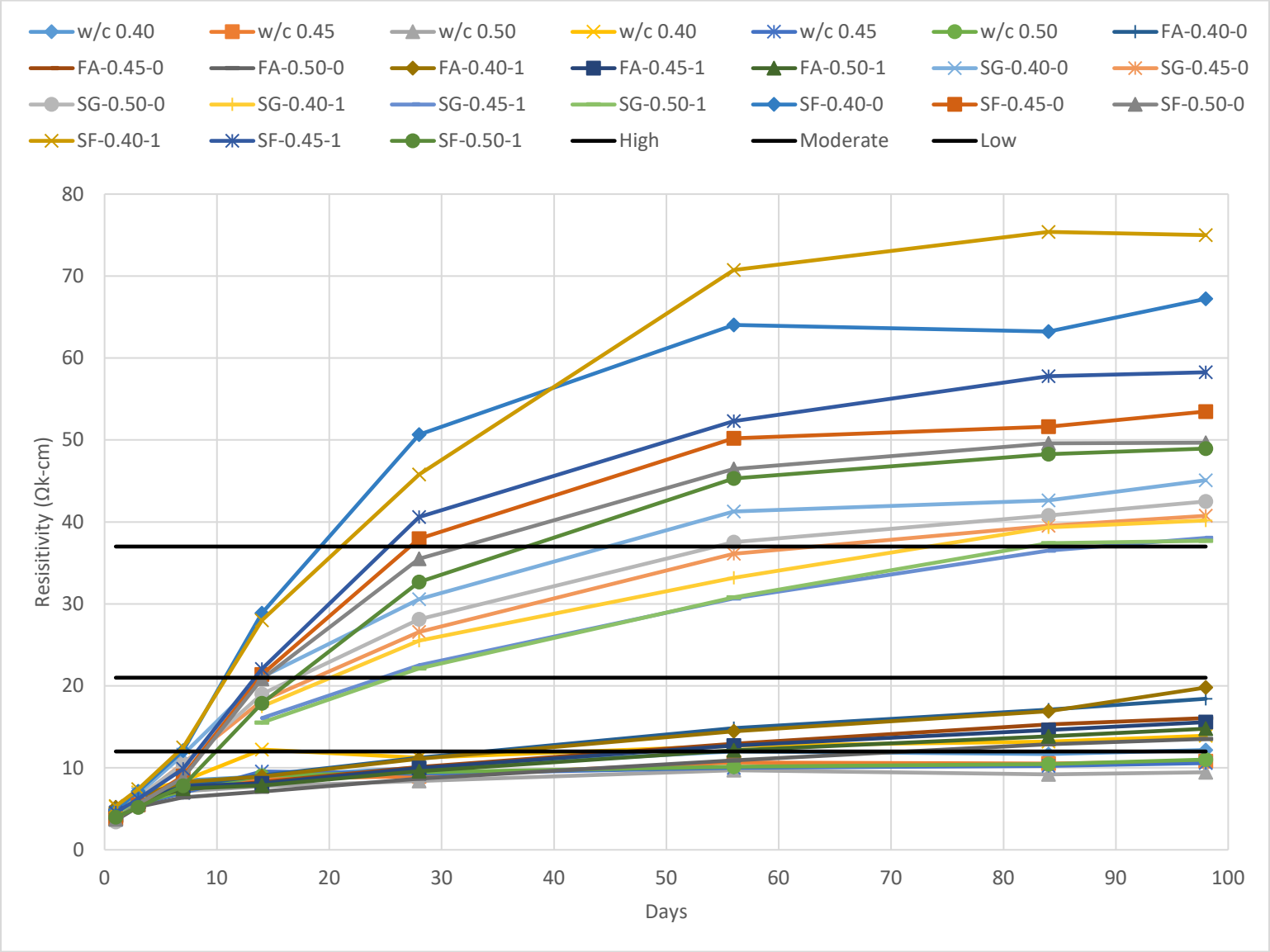

Figure 65. Graph. Gain in surface resistivity up to 98 days for all mixtures designs.

APPENDIX B: RESISTIVITY STUDY—MIXTURE DESIGN DETAILS

Table 9. Mixture Design Information for Mixture Containing 0% Fly Ash and 35% Slag Cement

	Resistivity (kΩ-cm)			Cement /Fly Ash / Slag Materials						3/4 in. Coarse Aggregate			1/2 in. or 3/8 in. Coarse Aggregate			Fine Aggregate				
MIX ID	28 Day	56 Day	91 Day	OPC (lb)	FA (lb)	SG (lb)	Total (lb)	FA (%)	SG (%)	CA1 (lb)	SpG	Abs (%)	CA2 (lb)	SpG	Abs (%)	FA (lb)	FA SpG	Abs (%)	Air (%)	w/cm Ratio
16	15.6	18.5	23.3	468		83	551	0	15	1800	2.66	1.8				1392	2.67	1.8	5.5	0.40
05	20.1	27.0	29.7	530		135	665	0	20				1730	2.7	2.1	1263	2.69	1.1	6.5	0.38
17	19.8	26.0		347		188	535	0	35	1368	2.70	1.7	547	2.69	2.2	1260	2.66	1.1	6.5	0.40
21	17.0	23.5	27.7	347		188	535	0	35	1475	2.70	1.7	442	2.69	2.2	1268	2.67	1.6	6.5	0.40
19	19.7	25.6	31.5	347		188	535	0	35	1368	2.70	1.8	547	2.69	2.2	1251	2.67	1.2	6.5	0.40
20	20.2	30.1	35.7	347		188	535	0	35	1475	2.70	1.8	442	2.69	2.2	1268	2.67	1.6	6.5	0.40
23	22.9	30.0	36.8	345		190	535	0	36	1411	2.69	1.9	500	2.69	2.3	1275	2.67	1.2	6.5	0.40
22	19.6	25.9	31.5	347		188	535	0	35	1390	2.70	1.7	547	2.69	2.2	1260	2.69	1.7	6.5	0.40
29F	18.2	26.6	36.2	347	55	133	535	10	25	1408	2.69	1.9	414	2.69	2.3	1320	2.67	1.2	6.5	0.42
40	16.1	21.3	25.5	375	60	145	580	10	25	1386	2.70	1.7	522	2.69	2.2	1157	2.66	1.1	6.5	0.42
44	15.9	22.4		375	60	145	580	10	25	1386	2.70	1.7	522	2.69	2.2	1165	2.69	1.7	6.5	0.42
18	16.7	28.0	31.4	375	60	145	580	10	25	1478	2.70	1.8	465	2.69	2.2	1154	2.67	1.2	6.5	0.40
26F	17.6	28.2	36.3	405	65	155	625	10	25	1490	2.74	1.2	350	2.73	1.8	1179	2.69	1.8	6.5	0.41
28F	17.5	25.7	33.9	435	70	165	670	10	25	1460	2.74	1.2	320	2.73	1.8	1130	2.69	1.8	6.5	0.42
27	20.3	29.4	34.3	340	60	120	520	12	23	1500	2.70	1.8	450	2.68	2.5	1300	2.69	1.3	6.5	0.42
30	17.6	24.5	30.9	345	65	125	535	12	23	1500	2.70	1.8	450	2.68	2.5	1280	2.69	1.3	6.5	0.42
01	22.2	35.8	46.7	310	80	210	600	13	35	1238	2.68	1.8	590	2.70	1.6	1278	2.71	0.9	6.5	0.37
02	33.1	40.1	51.7	310	80	210	600	13	35	1260	2.68	1.8	540	2.70	1.6	1305	2.71	0.9	6.5	0.37
03	28.7	48.4	47.6	310	80	210	600	13	35	1369	2.71	1.6	441	2.70	2.1	1303	2.69	1.1	6.5	0.37
04	29.1	41.6	51.8	310	80	210	600	13	35	1712	2.74	1.2	125	2.73	1.5	1289	2.67	1.6	6.5	0.37
46	15.6	25.6	35.1	320	75	100	495	15	20	1459	2.69	1.9	420	2.69	2.3	1327	2.67	1.6	6.0	0.46
45	15.7	26.4	38.0	345	80	110	535	15	21	1420	2.69	1.9	429	2.69	2.3	1308	2.67	1.6	6.0	0.43
24	19.0	27.1	31.6	345	80	110	535	15	21	1911	2.69	1.9				1251	2.67	1.6	6.5	0.40
37	17.8	26.1	31.8	374	81	120	575	14	21	1400	2.66	1.8	400	2.70	2.1	1265	2.68	1.8	6.5	0.42
35	14.9	20.8	27.6	374	81	120	575	14	21	1420	2.71	1.8	390	2.70	1.7	1270	2.64	1.5	6.5	0.42
34	17.3			374	81	120	575	14	21	1420	2.70	1.8	390	2.70	1.7	1270	2.64	1.5	6.5	0.42
38	13.7	17.7	24.6	374	81	120	575	14	21	1430	2.71	1.8	390	2.70	1.6	1280	2.62	1.9	6.5	0.42

	Resistivity (kΩ-cm)			Cement /Fly Ash / Slag Materials						3/4 in. Coarse Aggregate			1/2 in. or 3/8 in. Coarse Aggregate			Fine Aggregate				
MIX ID	28 Day	56 Day	91 Day	OPC (lb)	FA (lb)	SG (lb)	Total (lb)	FA (%)	SG (%)	CA1 (lb)	SpG	Abs (%)	CA2 (lb)	SpG	Abs (%)	FA (lb)	FA SpG	Abs (%)	Air (%)	w/cm Ratio
07	15.1	21.9	28.3	375	90	115	580	16	20	1667	2.70	1.7	250	2.69	2.2	1213	2.67	1.6	6.0	0.39
06	16.0	22.5	34.9	375	90	115	580	16	20	1667	2.70	1.8	250	2.69	2.2	1213	2.67	1.6	6.0	0.39
41	17.8	30.0	41.6	375	90	115	580	16	20	1733	2.70	1.8	216	2.69	2.3	1133	2.67	1.6	6.0	0.42
25	20.7	29.3	38.5	370	90	120	580	16	21	1630	2.69	2.4	264	2.68	2.3	1160	2.64	1.1	6.5	0.41
31	17.8	28.1	34.3	394	85	126	605	14	21	1399	2.70	1.5	376	2.70	1.6	1235	2.63	1.3	6.5	0.42
39	15.5	24.1	25.3	395	90	120	605	15	20	1366	2.70	1.7	514	2.69	2.2	1141	2.66	1.1	6.5	0.42
36	14.4	21.0	26.6	395	90	120	605	15	20	1606	2.70	1.7	243	2.69	2.2	1184	2.67	1.6	6.0	0.42
43	17.9	25.0	33.5	395	90	120	605	15	20	1606	2.70	1.8	243	2.69	2.2	1184	2.67	1.6	6.0	0.42
42	16.0	26.6	42.1	395	90	120	605	15	20	1764	2.69	1.9	182	2.69	2.3	1085	2.67	1.6	6.0	0.42
32	24.6	38.1		360	115	106	581	20	18	1630	2.70	1.7	260	2.69	2.2	1182	2.66	1.3	6.5	0.42
33	26.3	41.3		360	115	106	581	20	18	1630	2.70	1.7	260	2.69	2.2	1182	2.66	1.3	6.5	0.42
10	20.9	26.8	34.7	350	150	65	565	27	12	1340	2.68	1.8	500	2.70	1.6	1345	2.71	0.9	6.5	0.39
11	26.4	34.7	45.3	350	150	65	565	27	12	1340	2.68	1.8	500	2.70	1.6	1345	2.71	0.9	6.5	0.39
08	17.8	31.1	42.6	350	150	65	565	27	12	1385	2.68	1.9	458	2.70	1.7	1345	2.72	0.9	6.5	0.39
09	15.5	27.9	41.5	350	150	65	565	27	12	1385	2.68	1.9	458	2.70	1.7	1345	2.72	0.9	6.5	0.39
12	28.0			350	150	65	565	27	12	1392	2.71	1.6	445	2.70	2.1	1350	2.69	1.1	6.5	0.39
13	19.8	34.5		350	150	65	565	27	12	1392	2.71	1.6	448	2.70	2.1	1350	2.69	1.1	6.5	0.39
14	26.9	45.0	57.5	350	150	65	565	27	12	1733	2.74	1.2	135	2.73	1.5	1335	2.67	1.6	6.5	0.39
15	23.6	38.9	51.4	350	150	65	565	27	12	1733	2.74	1.2	135	2.73	1.5	1335	2.67	1.6	6.5	0.39


Illinois Department
of Transportation


ILLINOIS